

ATTACHMENT M



Reax Engineering Inc.
Job # 19-0739

Quantitative Wildfire Risk Analysis of the Klamath River Renewal Project - Preliminary Assessment

Prepared for Klamath River Renewal Corporation

Revision 0
February 26, 2020

Document Revision History



| Job # | Job Name | Client |
|--------------|---|-----------------------------------|
| 19-0739 | Quantitative Wildfire Risk Analysis of the Klamath River Renewal Project - Preliminary Assessment | Klamath River Renewal Corporation |

| Revision # | Date | Description | |
|-------------------|-------------------|---|---|
| Rev 0 | February 26, 2020 | Interim draft provided for KRRC review and comment. | |
| | | Prepared by: Chris Lautenberger Darrell Schulte Delaney Seeburger Maria Theodori | Approved by: Chris Lautenberger |
| | | | |
| | | Prepared by: | Approved by: |
| | | | |
| | | Prepared by: | Approved by: |
| | | | |
| | | Prepared by: | Approved by: |
| | | | |
| | | Prepared by: | Approved by: |
| | | | |

TABLE OF CONTENTS

| | |
|--|-----------|
| 1.0 INTRODUCTION..... | 1 |
| 2.0 BACKGROUND..... | 2 |
| 2.1 FIRE MANAGEMENT PLAN | 2 |
| 2.2 ANALYSIS AREA AND AERIAL SUPPRESSION EXTENT | 2 |
| 3.0 FIRE HISTORY..... | 4 |
| 3.1 FIRE OCCURRENCE | 4 |
| 3.1.1 Human-caused fires | 4 |
| 3.1.2 Lightning-caused fires | 7 |
| 3.1.3 Fires from all causes | 9 |
| 3.2 FIRE PERIMETERS | 10 |
| 3.3 LARGE FIRES OCCURRING IN ANALYSIS AREA | 14 |
| 3.3.1 2014 Oregon Gulch Fire | 14 |
| 3.3.2 2018 Klamathon Fire | 14 |
| 3.4 SUMMARY..... | 15 |
| 4.0 ANALYSIS OF PROPOSED FIRE MITIGATION MEASURES | 16 |
| 4.1 DETECTION EFFECTIVENESS..... | 16 |
| 4.1.1 Proposed post-removal fire detection scheme | 16 |
| 4.1.2 Alternative proposed fire detection scheme..... | 20 |
| 4.1.3 Limitations of viewshed analysis..... | 24 |
| 4.1.4 Satellite-based fire detection technology | 25 |
| 4.1.5 Recommendations for enhanced detection effectiveness | 26 |
| 4.2 SUPPRESSION EFFECTIVENESS | 26 |
| 4.2.1 Pre-restoration..... | 26 |
| 4.2.2 Post-restoration | 26 |
| 4.2.3 Quantification methodology | 26 |
| 4.2.4 Conclusions and next steps | 28 |
| 5.0 MONTE-CARLO FIRE SPREAD MODELING | 32 |
| 5.1 MONTE-CARLO FIRE SPREAD MODEL: ELMFIRE | 32 |
| 5.2 FUELS | 34 |
| 5.2.1 Pre-restoration..... | 34 |
| 5.2.2 Post-restoration | 35 |
| 5.3 FIRE WEATHER | 38 |
| 5.3.1 Methodology | 38 |
| 5.4 STOCHASTIC SELECTION OF IGNITION LOCATIONS AND WIND/WEATHER CONDITIONS | 40 |
| 5.5 BURN PROBABILITY OUTPUTS | 41 |
| 6.0 CONCLUSIONS AND NEXT STEPS..... | 44 |
| 7.0 REFERENCES..... | 45 |

LIST OF FIGURES

| | |
|--|----|
| FIGURE 1. LOCATION OF DAMS IN RELATION TO ANALYSIS AREA. | 3 |
| FIGURE 2. AERIAL SUPPRESSION EXTENT..... | 3 |
| FIGURE 3. HUMAN-CAUSED IGNITIONS IN ANALYSIS AREA. BLUE CIRCLES ARE PROJECT DAMS. | 5 |
| FIGURE 4. HUMAN-CAUSED FIRES IGNITION DENSITY. BLUE CIRCLES ARE PROJECT DAMS. | 5 |
| FIGURE 5. HUMAN-CAUSED FIRES IGNITION DENSITY AND ROAD NETWORK. | 6 |
| FIGURE 6. HUMAN-CAUSED FIRES IGNITION DENSITY AND BUILDING FOOTPRINTS. | 6 |
| FIGURE 7. LIGHTNING-CAUSED IGNITIONS IN ANALYSIS AREA..... | 8 |
| FIGURE 8. LIGHTNING-CAUSED FIRES IGNITION DENSITY..... | 8 |
| FIGURE 9. LIGHTNING CAUSED FIRES IGNITION DENSITY AND TERRAIN. | 9 |
| FIGURE 10. IGNITION DENSITY – ALL CAUSES. | 10 |
| FIGURE 11. CALIFORNIA FIRE PERIMETERS 1970-1979..... | 11 |
| FIGURE 12. CALIFORNIA FIRE PERIMETERS 1980-1989..... | 11 |
| FIGURE 13. CALIFORNIA FIRE PERIMETERS 1990-1999..... | 12 |
| FIGURE 14. CALIFORNIA FIRE PERIMETERS 2000-2009..... | 12 |
| FIGURE 15. CALIFORNIA FIRE PERIMETERS 2010-2019..... | 13 |
| FIGURE 16. OREGON FIRE PERIMETERS 2000-2019..... | 13 |
| FIGURE 17. FINAL PERIMETER OF THE 2014 OREGON GULCH FIRE..... | 14 |
| FIGURE 18. FINAL PERIMETER OF THE 2018 KLAMATHON FIRE. | 15 |
| FIGURE 19. MDS CAMERA LOCATIONS FOR POST-REMOVAL FIRE DETECTION. | 17 |
| FIGURE 20. POST-REMOVAL FIRE DETECTION VIEWSHED ANALYSIS. | 19 |
| FIGURE 21. POST-REMOVAL FIRE DETECTION CAMERA VIEWSHED ANALYSIS OVERLAID WITH THE AERIAL SUPPRESSION EXTENT. | 20 |
| FIGURE 22. PROPOSED MDS CAMERA LOCATIONS FOR FIRE DETECTION INCLUDING MT. ASHLAND..... | 22 |
| FIGURE 23. RESULTS OF THE VIEWSHED ANALYSIS FOR THE ALTERNATE PROPOSED CAMERA SCHEME OVERLAID WITH THE AERIAL SUPPRESSION EXTENT..... | 22 |
| FIGURE 24. POST-REMOVAL VIEWSHED ANALYSIS EMPHASIZING MT. ASHLAND CONTRIBUTION..... | 23 |
| FIGURE 25. VIEWSHED OF REGION BETWEEN PARADISE CRAGGY AND EAGLE ROCK..... | 24 |
| FIGURE 26. SMOKE PLUME DETECTION FROM A CAMERA IN THE ALERTWILDFIRE NETWORK [15]..... | 25 |
| FIGURE 27. POST-REMOVAL MANAGEMENT RESOURCES PROVIDED AS PART OF THE LONG-TERM FMP [6]. | 29 |
| FIGURE 28. PRE- AND POST-RESTORATION DIP SITES..... | 30 |
| FIGURE 29. RIGID TANK MODEL SHOWN WITH HELICOPTER SNORKEL. | 31 |
| FIGURE 30. SOFT-SIDED TANK MODEL BEING AIRLIFTED. | 31 |
| FIGURE 31. SAMPLE ELMFIRE FIRE SPREAD SIMULATION FOR INDIVIDUAL FIRE IGNITION. (A) FIRE TYPE (SURFACE FIRE, PASSIVE CROWN FIRE, OR ACTIVE CROWN FIRE). (B) FLAME LENGTH. | 33 |
| FIGURE 32. IRON GATE AND COPCO SURFACE FUEL PRE-RESTORATION | 35 |
| FIGURE 33. FCCS EXISTING VEGETATION TYPES..... | 36 |
| FIGURE 34. LANDFIRE 2.0.0 (REMAP) EXISTING VEGETATION TYPES. | 36 |
| FIGURE 35. IRON GATE AND COPCO SURFACE FUELS POST-RESTORATION..... | 37 |
| FIGURE 36. KRRC ANALYSIS AREA AND IGNITION MASK. | 40 |
| FIGURE 37. PRE-RESTORATION BURN PROBABILITY. | 42 |
| FIGURE 38. POST-RESTORATION BURN PROBABILITY..... | 42 |
| FIGURE 39. DIFFERENCE BETWEEN PRE- AND POST-RESTORATION BURN PROBABILITY. | 43 |

LIST OF TABLES

| | |
|--|----|
| TABLE 1. POST-REMOVAL MDS CAMERA LOCATIONS..... | 17 |
| TABLE 2. CAMERA VIEWSHED ANALYSIS INPUTS..... | 18 |
| TABLE 3. ALTERNATE MDS CAMERA LOCATIONS WITH ADDITIONAL LOCATIONS SHOWN IN GRAY..... | 21 |
| TABLE 4. ALTERNATE CAMERA VIEWSHED ANALYSIS INPUTS..... | 21 |
| TABLE 5. IMPROVED EAGLE ROCK VIEWSHED ANALYSIS SITING..... | 21 |
| TABLE 6. IGNITION PROBABILITY BY WOODY EMBERS/FIREBRANDS AS TABULATED BY SCHROEDER [51]..... | 39 |

1.0 INTRODUCTION

Reax Engineering Inc. (Reax) has been retained by the Klamath River Renewal Corporation (KRRC) to quantify the change in fire risk associated with the removal of four dams along the Klamath River and adjacent areas where fire risk may change due to these restoration activities. In order to do so, climatological (long-term) fire risk must be quantified using an analysis that considers, among others, the following factors:

- Vegetation growth in areas that were previously reservoir,
- Reduction in the amount of water available for firefighting purposes,
- Change in land use including increased recreation,
- Removal of potential ignition sources associated with electrical generation, and
- Risk reduction/mitigation countermeasures such as real-time fire detection monitoring, introduction of additional water sources for ground crews, new firefighting equipment for local volunteer fire departments, and possibly fuel treatments.

Reax has developed a methodology that integrates weather modeling and Monte-Carlo simulation fire modeling to quantify geospatial fire risk. Here, risk is considered the product of fire occurrence probability and impacts to assets at risk such as communities/structures, timber, critical species habitat, and cultural resources. The basic methodology, which has been demonstrated to successfully identify areas susceptible to large-scale structure losses and has been applied to map utility-associated fire risk, is described later in this report and forms part of the basis of the work proposed here.

This report is organized as follows:

- Section 2 provides background information regarding the KRRC project.
- Section 3 describes fire history in the analysis area.
- Section 4 analyzes pre- and post-restoration state of the analysis area and the proposed changes in suppression and detection effectiveness.
- Section 5 prescribes the Monte-Carlo fire spread modeling methodology used to determine burn probabilities and quantify risk.
- Section 6 summarizes preliminary findings, recommendations, and next steps.

Due to the interim nature of this report, several aspects of the work described herein remain ongoing. This report is intended to provide a progress update to the KRRC on preliminary findings, recommendations, and subsequent next steps. A final report will be provided in April 2020.

2.0 BACKGROUND

2.1 Fire management plan

KRRC developed a draft Fire Management Plan (FMP) to address fire prevention and suppression associated with the physical removal of four hydroelectric dams along the Klamath River (Iron Gate, Copco No. 1, Copco No. 2, and J.C. Boyle). The goal of the FMP is to assure that the dam removals will not cause a net diminution in firefighting resources and that, both during and after demolition, the current fire ignition risk that exists will not increase as a result of the dam removal.

Pursuant to this goal, the FMP contains:

- Background on the history of fire in the region,
- Local fire agency jurisdictions and regulatory requirements,
- Descriptions of the short- and long-term FMPs to be implemented by KRRC.

Review and analysis of the FMP is the starting point for the work described in the current report.

2.2 Analysis area and aerial suppression extent

Analyzing fire risk in an area only immediately adjacent to the river course discounts the impact that removing the dams could have on fire risk at greater distances. Conversely, analyzing fire risk in areas at scales approaching the size of California and Oregon is inefficient. For that reason, the analysis area used in this project (Figure 1) is a 50-mile buffer surrounding the four dams slated for removal. The distance of 50-miles was chosen to strike a balance between analyzing an enormous region and capturing the extent of terrain that will be impacted by the dam removal.

The analysis area shown in Figure 1 is used primarily in the Monte-Carlo fire spread analysis (Section 5.0). However, a smaller area known as the Aerial Suppression Extent (ASE) is used as a boundary in the detection effectiveness analysis (Figure 2). The ASE was defined by CALFIRE and delineates the land area where water drafted from the existing reservoirs could be used in aerial fire suppression.

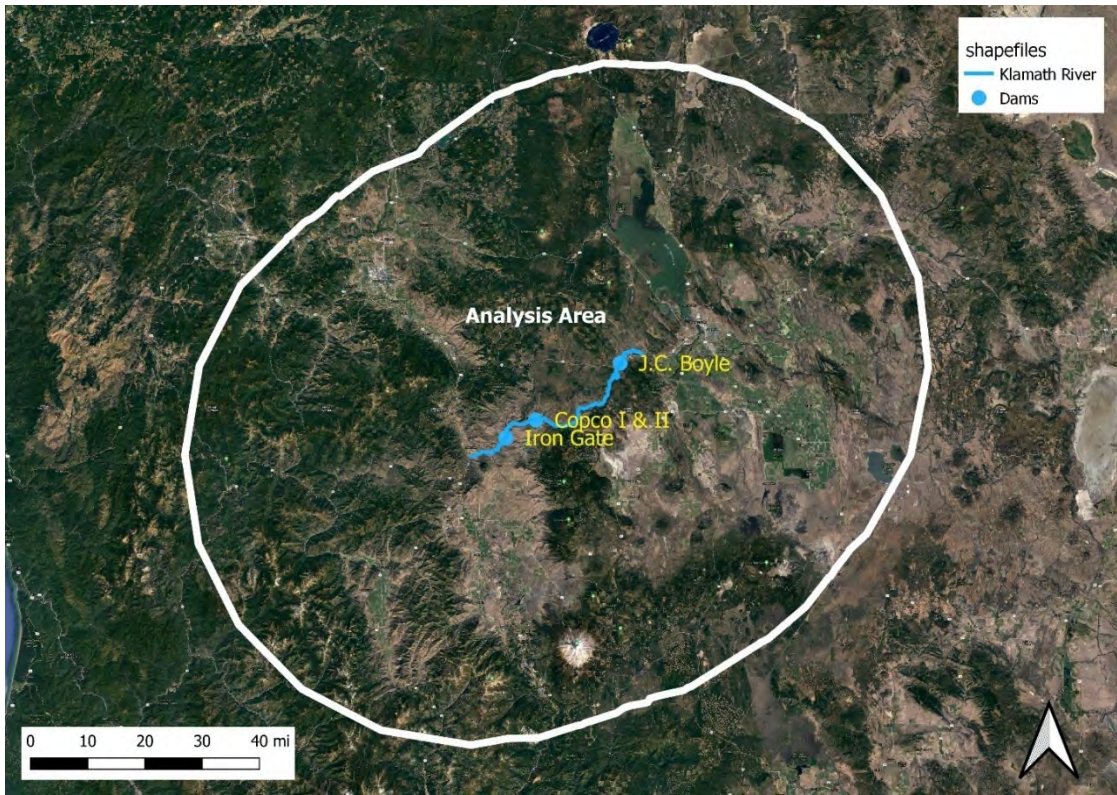


Figure 1. Location of dams in relation to analysis area.

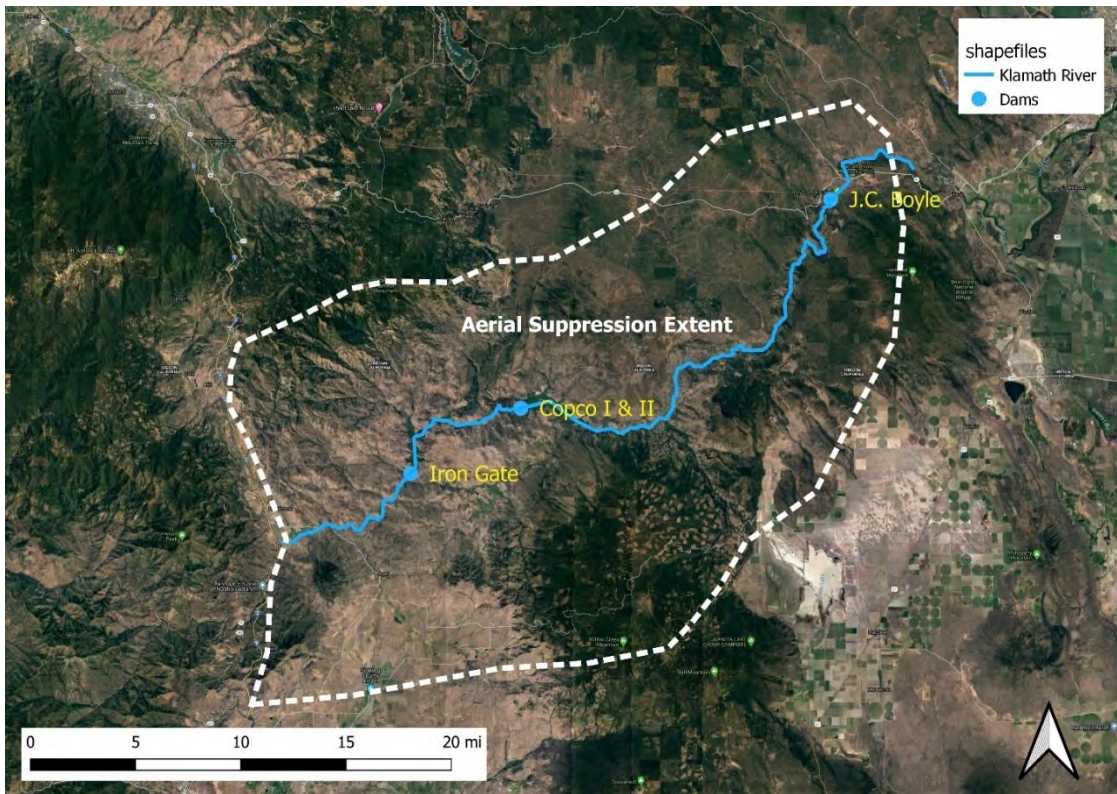


Figure 2. Aerial Suppression Extent.

3.0 FIRE HISTORY

To understand how fire has historically impacted the analysis area, fire history records for Oregon and California were aggregated and analyzed. Such analysis of past fire history provides context for expected fire sizes, locations, causes, and frequency at which fires occur. It can also provide insight into local hazards or weather events that dramatically influence fire behavior.

3.1 Fire occurrence

The US Forest service has published a Fire Occurrence Database (FOD) [1] which contains spatial information for wildfires in the United States between 1992 and 2015. Federal, state, and local fire organizations contributed records with minimum requirement that the records include discovery date, final fire size, and a point location accurate to 1-square mile. Where possible, data were transformed to meet the National Wildfire Coordinating Group's (NWCG) data standards. Error-checking was performed, and redundant records were removed where possible, resulting in a database with 1.88 million geo-referenced wildfire records. The FOD also records fire cause, allowing spatial and temporal distinctions to be made. The difference of greatest interest to the KRRC project is between human-caused and lightning-caused fires.

3.1.1 Human-caused fires

Human-caused fires describe a range of possible ignition causes including debris burning, vehicle, utility, and campfires, among others. The locations of these types of ignitions tend to follow linear features such as roads or be clustered near centers of human activity such as residential neighborhoods, campgrounds, etc. Human-caused ignition locations in the analysis area are shown in Figure 3. These individual ignition locations were used to create the ignition density "heatmap"¹ shown in Figure 4. Road networks and building footprints were overlaid on the heatmap to illustrate the concentration of ignitions near infrastructure (Figure 5, Figure 6).

Human-caused fires tend to be smaller and are more successfully suppressed in the initial attack than lightning-caused fires. However, these ignitions are of significant interest despite the higher probability of success in initial attack because large human-caused fires coincide with unusually high wind speeds, particularly in the western United States [2]. This can be attributed to many factors, including the expansion of human-caused ignitions into regions and during seasons where wind speeds are climatologically higher and the reduced tactical capacities of aerial suppression efforts during high winds [2].

¹ Created using inverse distance weighted kernel density

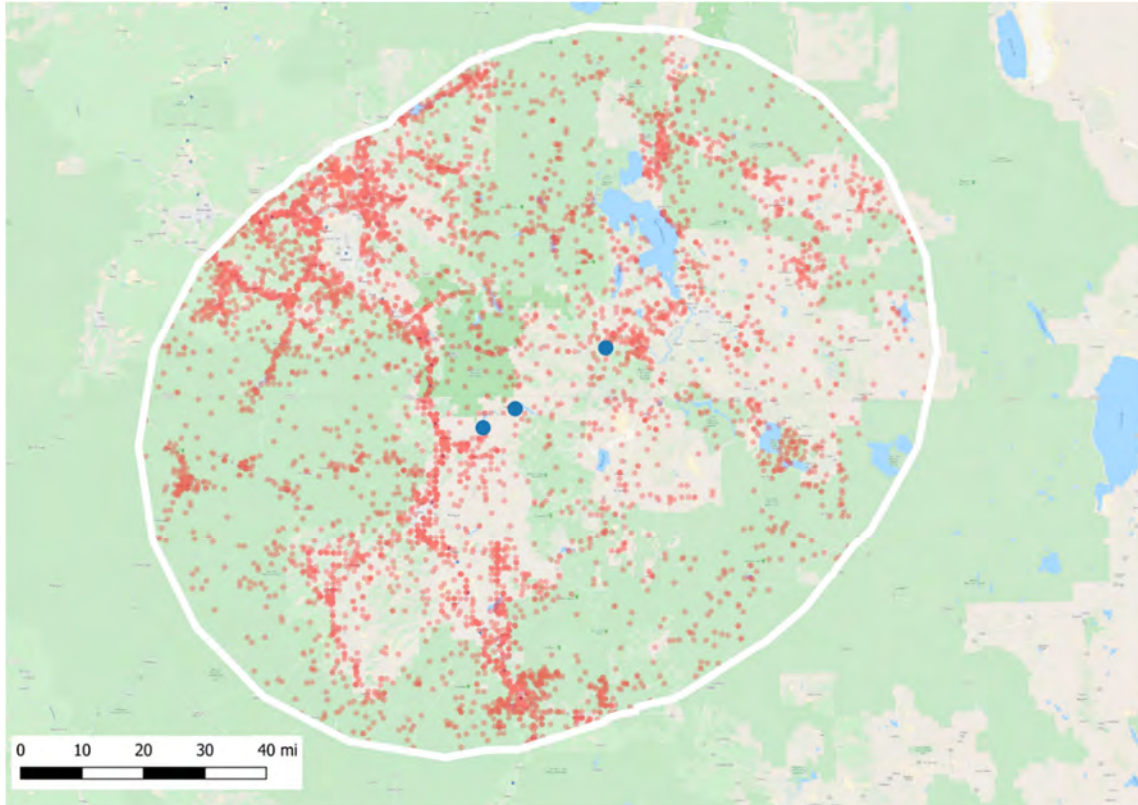


Figure 3. Human-caused ignitions in analysis area. Blue circles are project dams.

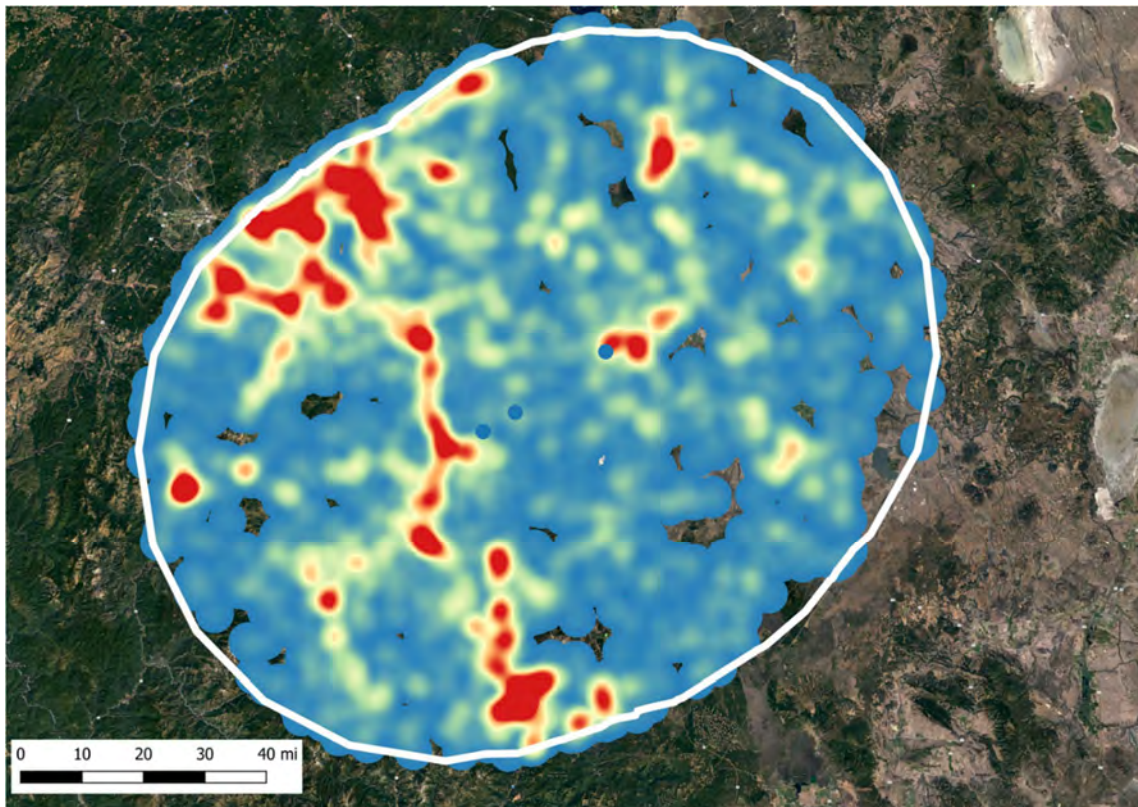


Figure 4. Human-caused fires ignition density. Blue circles are project dams.

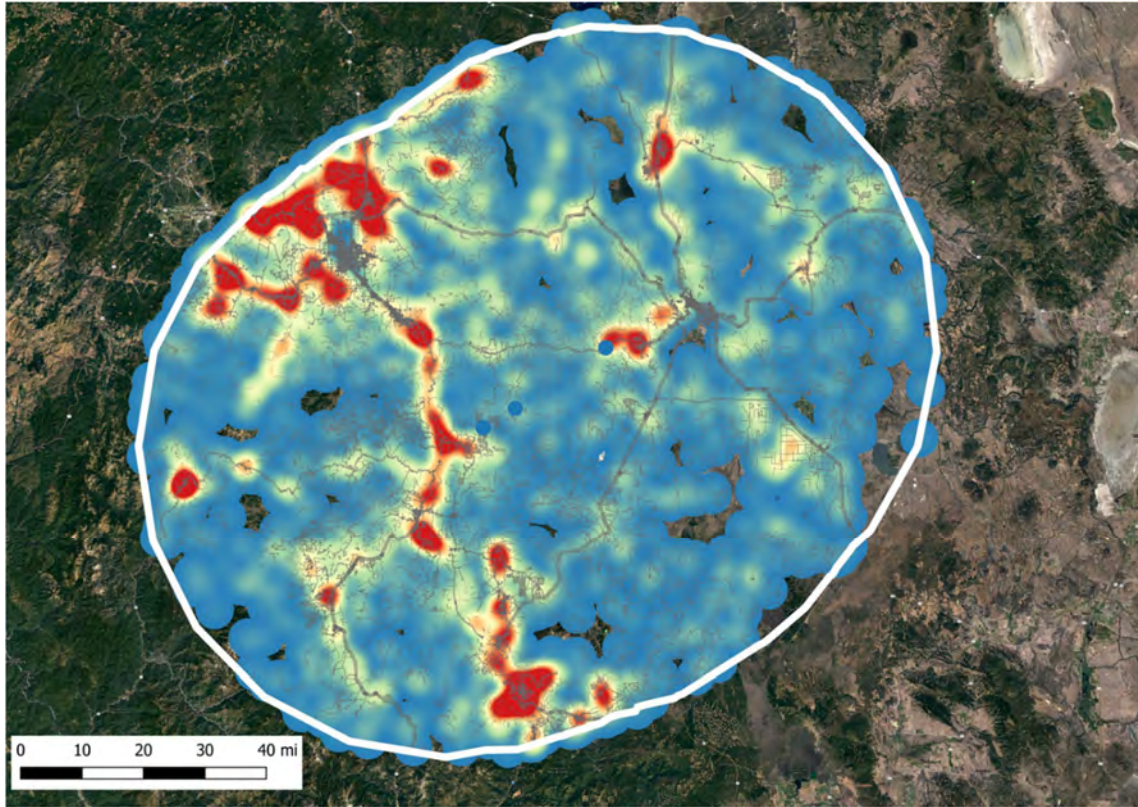


Figure 5. Human-caused fires ignition density and road network.

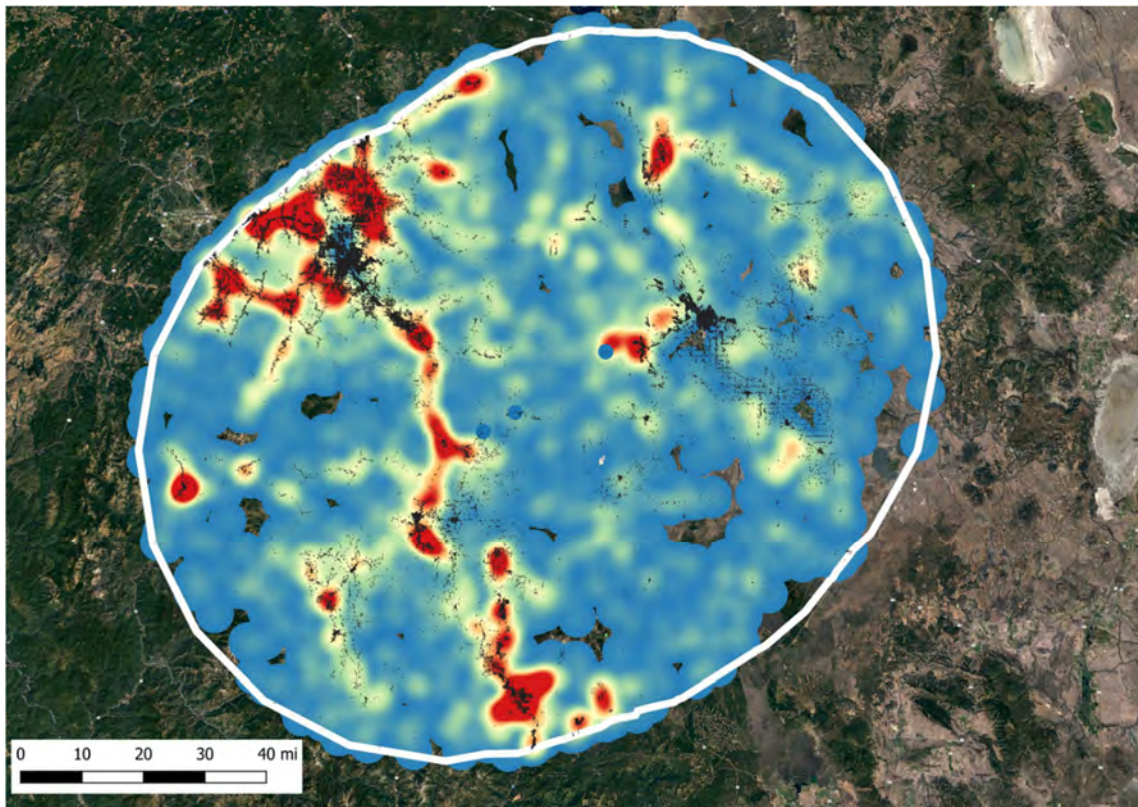


Figure 6. Human-caused fires ignition density and building footprints.

3.1.2 *Lightning-caused fires*

Locations of lightning-caused ignitions tend to be more randomly and uniformly distributed than human-caused fires (Figure 7). To show the relative location of lightning-caused ignitions with respect to topography, a heatmap was generated (Figure 8). The distribution of lightning-caused ignitions does not achieve the intense localization that human-caused ignitions exhibited. The lightning-caused fire heatmap is overlaid with a hill shade raster in Figure 9, allowing the correspondence between topography and lightning-caused ignitions to be visualized.

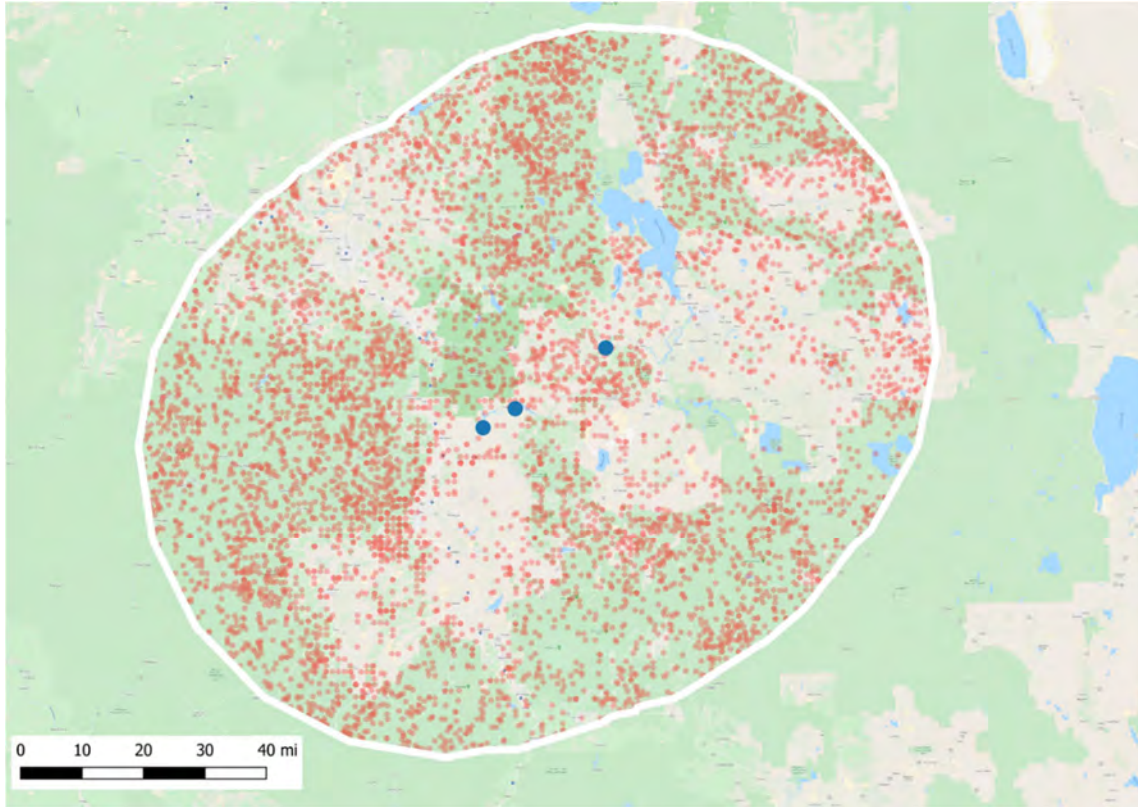


Figure 7. Lightning-caused ignitions in analysis area.

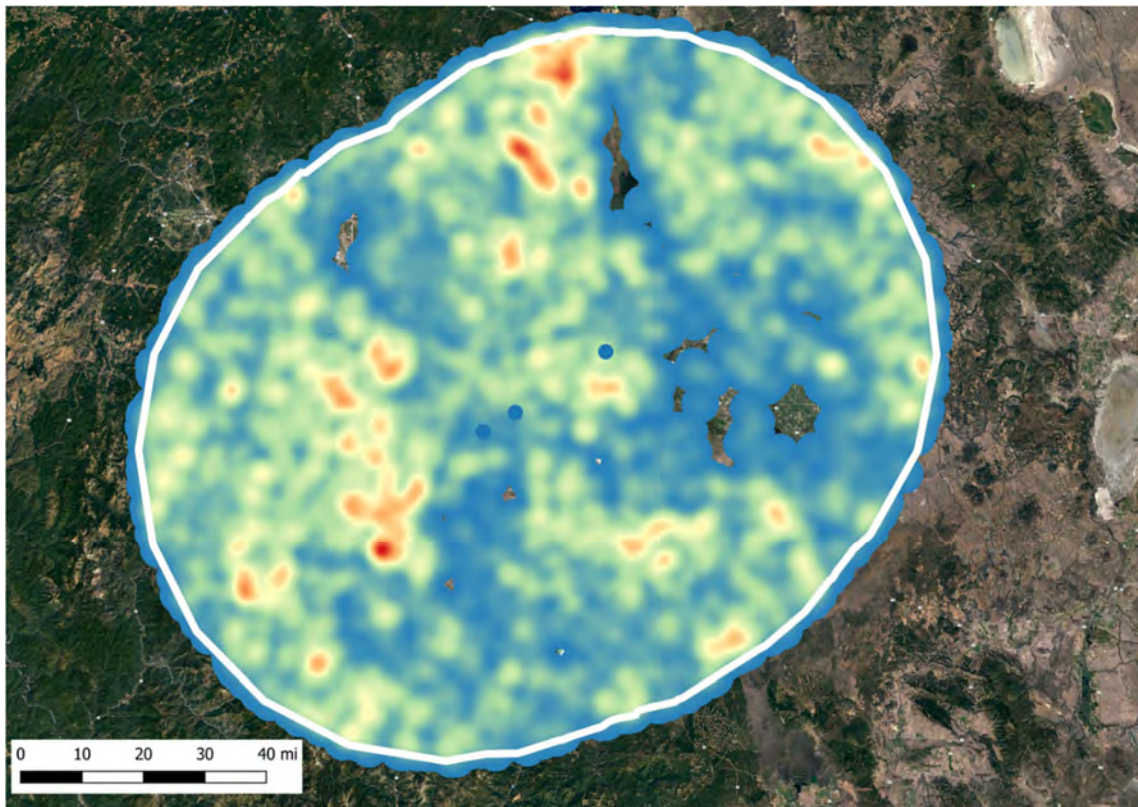


Figure 8. Lightning-caused fires ignition density.

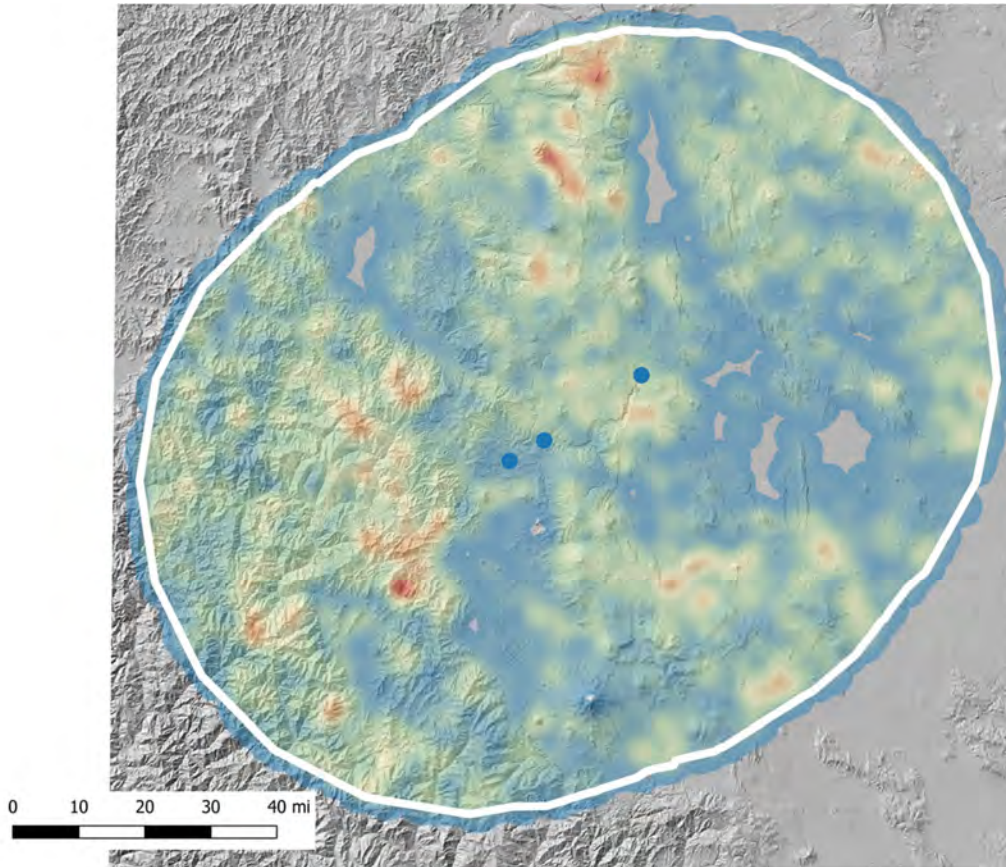


Figure 9. Lightning caused fires ignition density and terrain.

3.1.3 Fires from all causes

Compiling ignitions from human- and lightning-caused ignitions within the analysis area resulted in an additional heatmap (Figure 10). Trends from all ignitions are visible and can be traced back to the contributing cause. For example, the high-density along linear features reflects the human-caused ignitions while the increase in density across the entire analysis area can be ascribed primarily to lightning-caused ignitions.

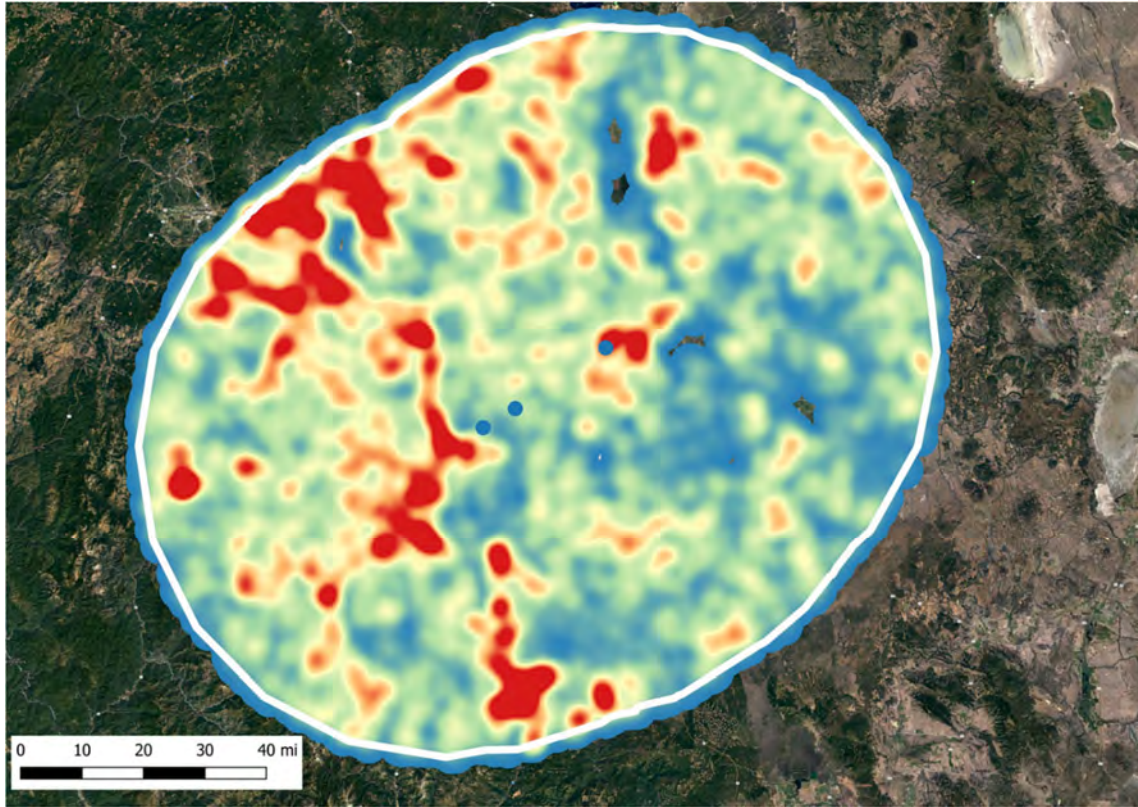


Figure 10. Ignition density – all causes.

3.2 Fire perimeters

Historical fire perimeters in California and Oregon were used to understand historical fire occurrence, particularly large fires, in the analysis area. The CALFIRE Fire and Resource Assessment Program (FRAP) database [3] was used for ultimate perimeters in California, GeoMAC data [4] was used ultimate perimeters in Oregon, and the National Interagency Fire Center (NIFC) [5] database was used to analyze daily progression of significant fires. Figure 11 - Figure 15 present fire perimeters from the FRAP database by decade from 1970 – 2018. Figure 16 presents perimeters in Oregon from 2000-2019 (the period of availability from GeoMAC).

Viewing the perimeters in context with the surrounding landscape shows that most fires in the analysis area have been small, indicating rapid response and effective containment from fire agencies relative to fire spread rates. There were, however, some notable exceptions. Several key larger fires were examined in greater detail to understand the conditions that led to such extensive growth. As part assessing these large historical fires, documentation on suppression resources used by local fire agencies in containing the fires were reviewed because fire agencies have expressed concern over the availability of water for aerial suppression efforts.

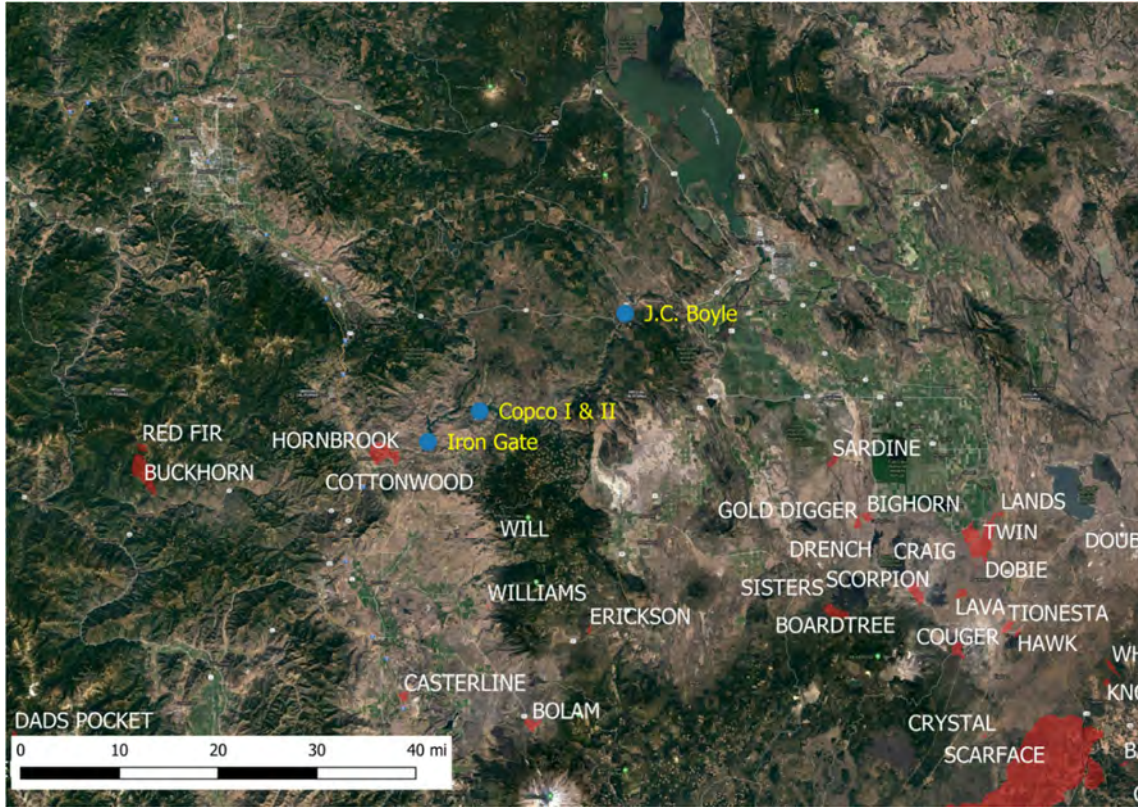


Figure 11. California fire perimeters 1970-1979.

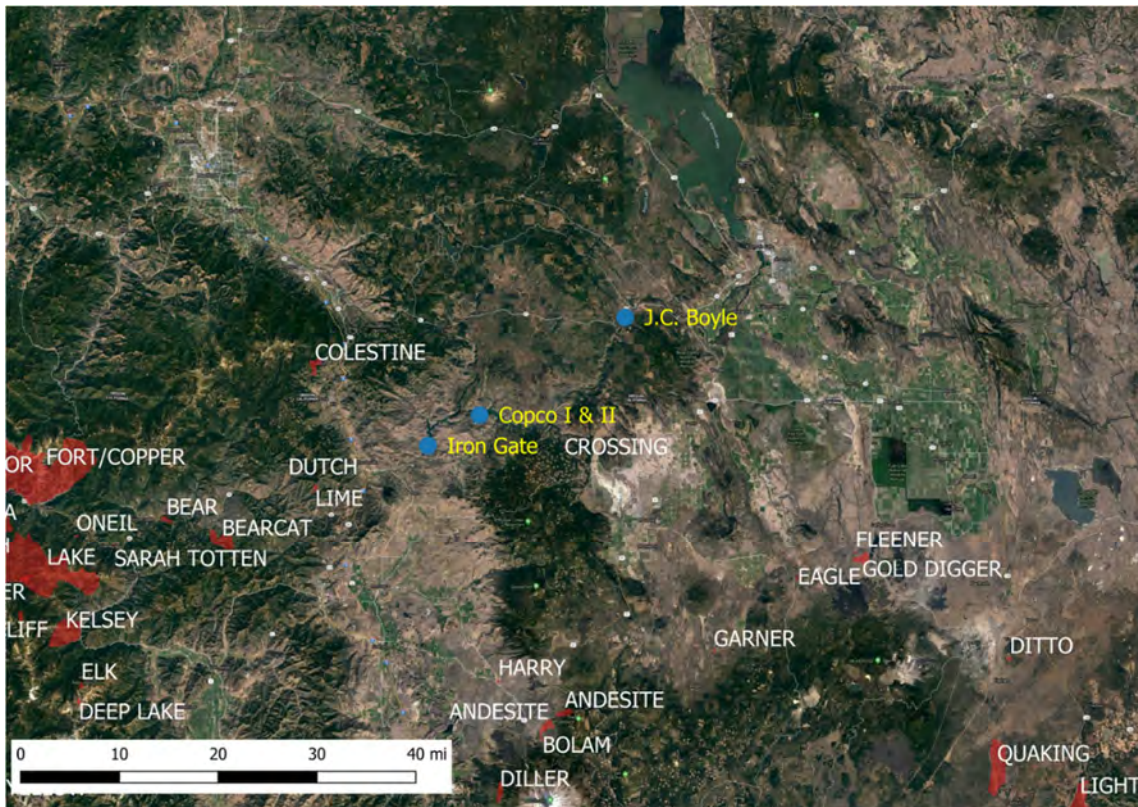


Figure 12. California fire perimeters 1980-1989.

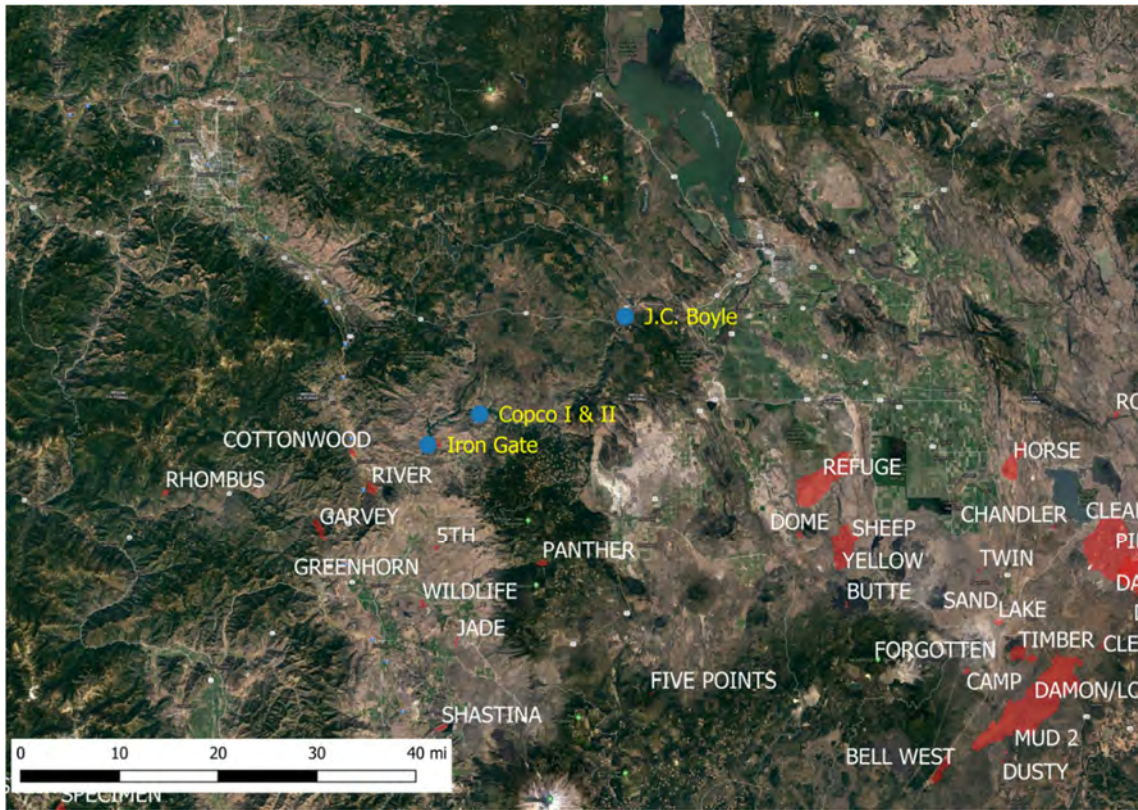


Figure 13. California fire perimeters 1990-1999.

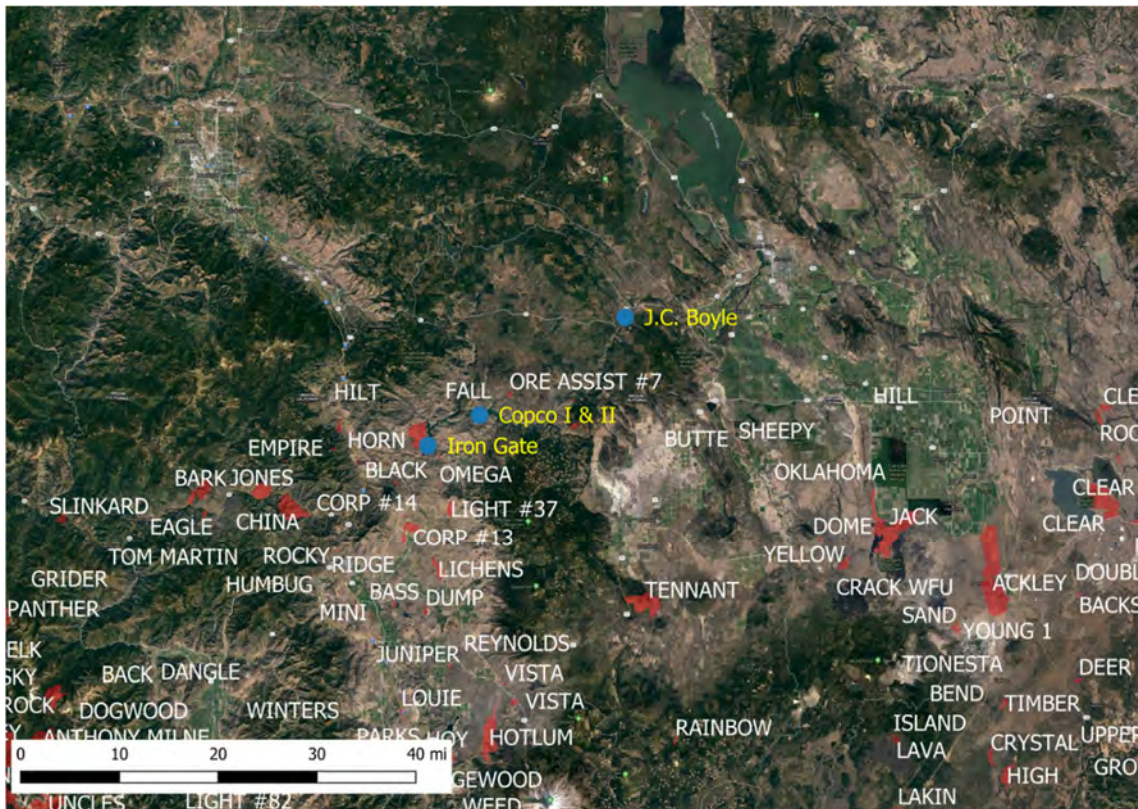


Figure 14. California fire perimeters 2000-2009.

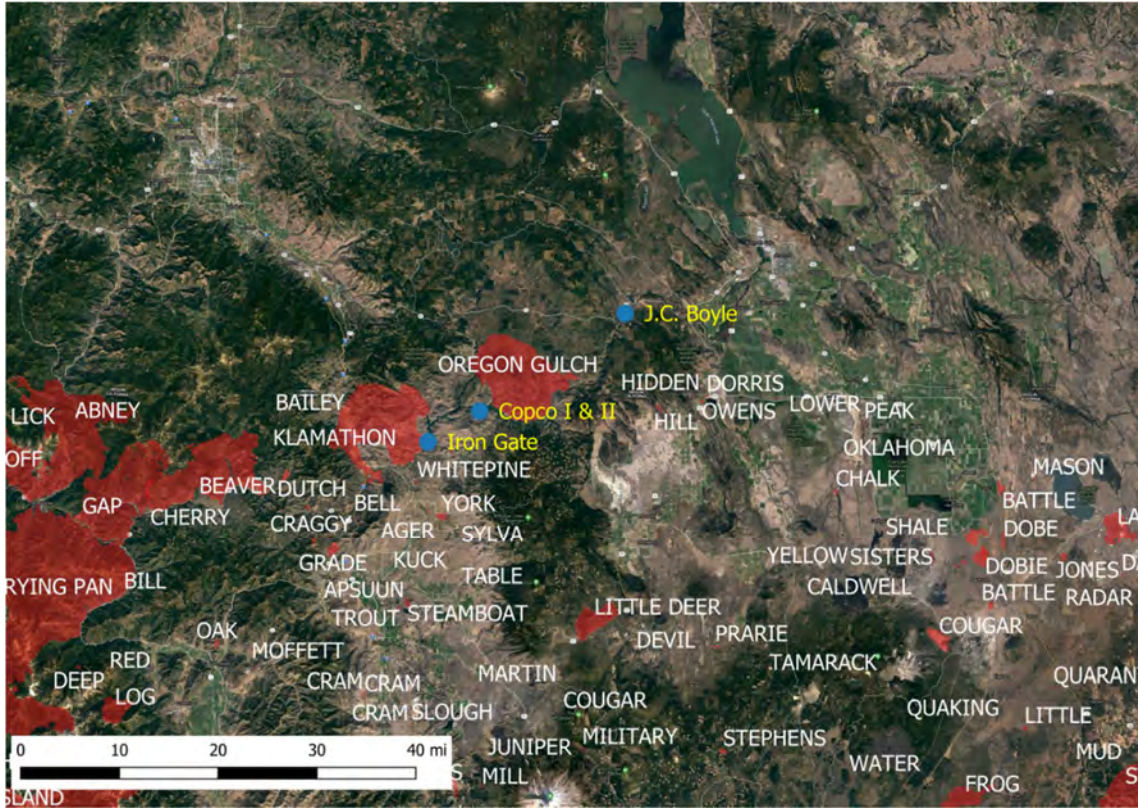


Figure 15. California fire perimeters 2010-2019.

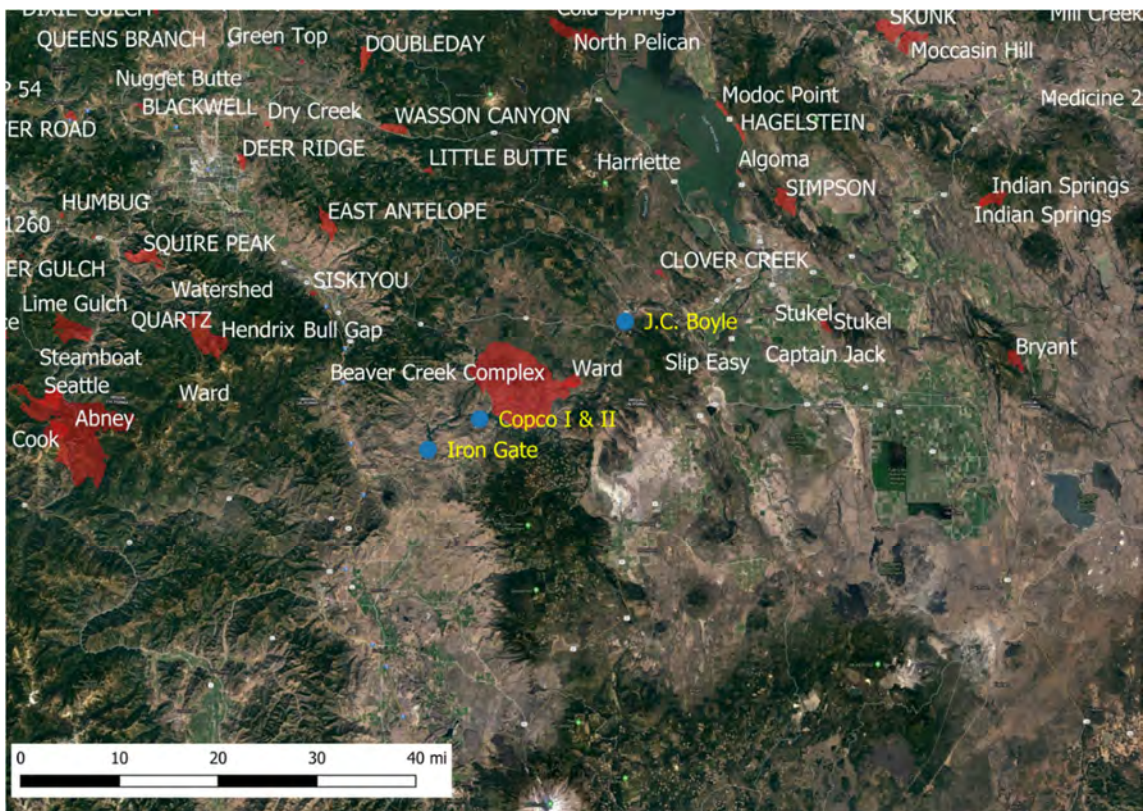


Figure 16. Oregon fire perimeters 2000-2019.

3.3 Large fires occurring in analysis area

As part of the analysis, fire weather conditions associated with historically significant fires in the analysis area surrounding the analysis area were evaluated. The two most significant fires occurring in the analysis area within the last ten years are the 2014 Oregon Gulch Fire (Section 3.3.1) and the 2018 Klamathon Fire (Section 3.3.2).

3.3.1 2014 Oregon Gulch Fire

The Oregon Gulch Fire was ignited on Thursday, July 30, 2014 from a lightning strike. By Friday morning the fire had grown to 7,500 acres. Over the course of two weeks, the fire burned a total of 35,111 acres north and east of the Copco dams. Figure 17 shows approximately daily progression from infrared imaging and satellite fire detection. The southern edge of the fire advanced up to the Klamath River. Oregon Gulch was managed as part of the Beaver Creek Complex and was declared 100% contained on August 13, 2014.

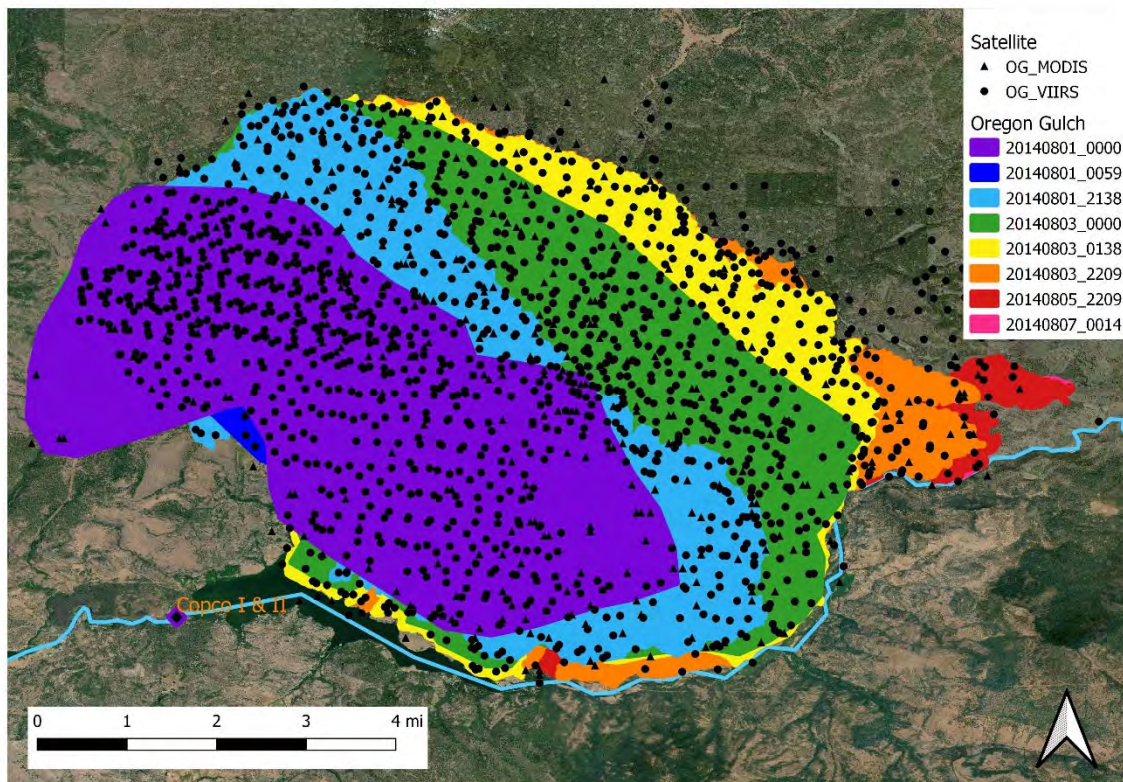


Figure 17. Final perimeter of the 2014 Oregon Gulch Fire.

3.3.2 2018 Klamathon Fire

The Klamathon Fire was reported on July 5, 2018, near Hornbrook, CA. By the following evening the fire had grown to 9,600 acres. Aerial suppression efforts relied on five dip sites, two from the reservoir above Iron Gate dam, one from the Klamath river, and two from runoff ponds. The Incident Action Plans (IAP) available from the National Interagency Fire Center (NIFC) database [5] did not contain ICS 209 forms so the exact tactics and number of drops was not able to be

determined from publicly-available data. The ICS 220 forms that were available provided the type of resource and time at which the resource began operating each day. The communities of Hornbrook, Hilt, and Colestin were evacuated in addition to the area around Iron Gate dam. By July 21, 2018, the fire was reported as contained having burned 38,008 acres (Figure 18). There was one civilian fatality and three non-fatal injuries resulting from the fire. At least 80 structures were damaged or destroyed.

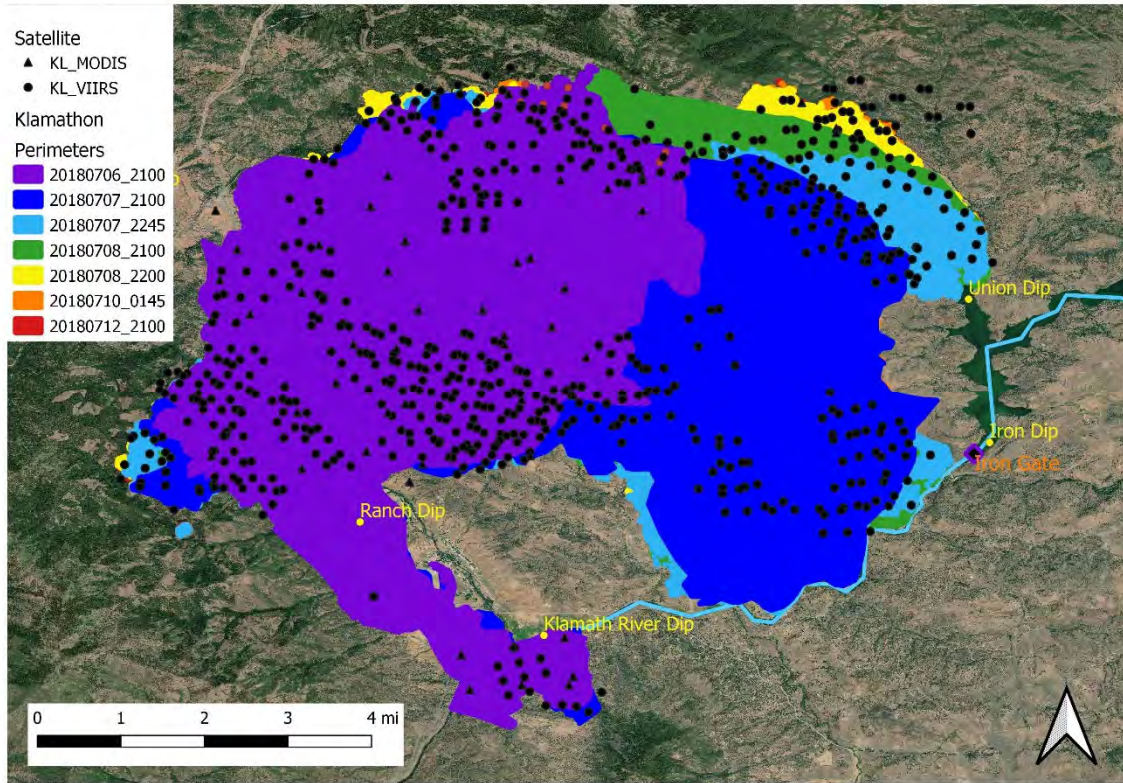


Figure 18. Final Perimeter of the 2018 Klamathon Fire.

3.4 Summary

The historical fire perimeters show that most fires in the analysis area were small with some exceptions. The Oregon Gulch and Klamathon fires were examined in greater detail to understand the conditions surrounding their rapid expansion. Where available, documentation and data regarding aerial suppression were reviewed and analyzed to address the concerns of local fire agencies with respect to the proposed dam removal and its impact on available water sources.

4.0 ANALYSIS OF PROPOSED FIRE MITIGATION MEASURES

The FMP [6] addresses long-term fire management in the Klamath River Basin, incorporating strategies to offset the loss of the three Klamath River reservoirs which have supported fire suppression resources in the past. The FMP also elaborates on the long-term new local and regional fire suppression resources to be implemented in the Basin. KRRC has committed to implement (and oversee through license surrender) effective and feasible strategies and concepts to enhance both short- and long-term fire prevention, detection, and suppression in the Basin. The focus of the analyses described in the current report is change in detection effectiveness (Section 4.1) and suppression effectiveness (Section 4.2).

4.1 Detection effectiveness

Despite best efforts in fire prevention, it is not possible to stop all fire ignitions from occurring. Therefore, the primary goal of a fire management plan is to minimize the likelihood of large-scale fire development such that a fire does not become too difficult to suppress or contain. A critical component of the overall strategy is reliable, rapid fire detection following an ignition, including accurately placing the ignition location and prompt notification of responding authorities. The shorter the length of time between fire start and fire detection, the higher the probability of a successful initial attack. In the past, fires were commonly spotted and reported by personnel at staffed fire lookout towers. Today there are various methods of detection and new technologies available such as the use of sensors, cameras, and satellites.

In California and Oregon, there has been an increase in detection camera installations at fire lookouts that were historically staffed. Fire size at the time of detection by cameras generally scales with distance from the camera, allowing fires to be detected at much smaller sizes than are possible with the human eye alone. ODF reports that it is possible for a camera to detect fires on the order of 1/100th of an acre within 10 miles. Beyond 10 miles, cameras can typically detect fires at 1/10th of an acre.

Existing fire detection resources and the proposed post-removal resources provided in the Klamath River Basin are discussed in detail in the FMP and are summarized here. A viewshed analysis identifies areas on Earth's surface that are visible from a specific location [7, 8] and is used in this work to:

1. Determine if the proposed post-removal resources provide adequate detection coverage of the protected areas of the Klamath River Basin, and
2. Quantify the change in detection effectiveness between pre- and post-removal schemes.

4.1.1 *Proposed post-removal fire detection scheme*

As described in the FMP, the post-removal fire detection scheme involves a Monitored Detection System (MDS) consisting of five planned or existing towers equipped with video surveillance cameras for around-the-clock, remote fire monitoring. The MDS technology transmits high definition video and images from cameras to an integrated GIS platform that is monitored by dedicated staff. The software that enables this integration is EnviroVision Solutions (EVS)

ForestWatch [9]. The same software also enables triangulation of the location of a fire if more than one camera captures the fire.

The cameras that are recommended by EVS for use with the ForestWatch system are industrial Pelco cameras that can automatically rotate 360°, have an auto-detection surveillance distance of up to 12.4 miles (20 kilometers), and can be manually and remotely controlled. The infrared and near-infrared capabilities allow the cameras to see through haze and nighttime conditions. The five towers where the MDS cameras would be located and the tower specifications are detailed below (Table 1 and Figure 19).

Table 1. Post-removal MDS camera locations.

| <i>Tower Name/Location</i> | <i>Elevation (ft)</i> | <i>Tower Height^a (ft)</i> | <i>Longitude</i> | <i>Latitude</i> |
|------------------------------|-----------------------|--------------------------------------|------------------|-----------------|
| Paradise Craggy, CA | 4,890 | 6 | -122.54669 | 41.81476 |
| Parker Mountain, OR | 5,165 | 50 | -122.27865 | 42.10527 |
| Chase Mountain, OR | 6,349 | 20 | -121.99415 | 42.09461 |
| Soda Mountain, OR | 6,049 | 10 | -122.47882 | 42.06447 |
| Eagle Rock ^b , CA | 6,863 | 10 | -122.24536 | 41.88152 |

^a Tower heights were determined from online resources [10-13]

^b This tower is not yet constructed. The elevation and location coordinates are approximated from GIS data provided to Reax. A conservative tower height was assumed based on the heights of existing towers.

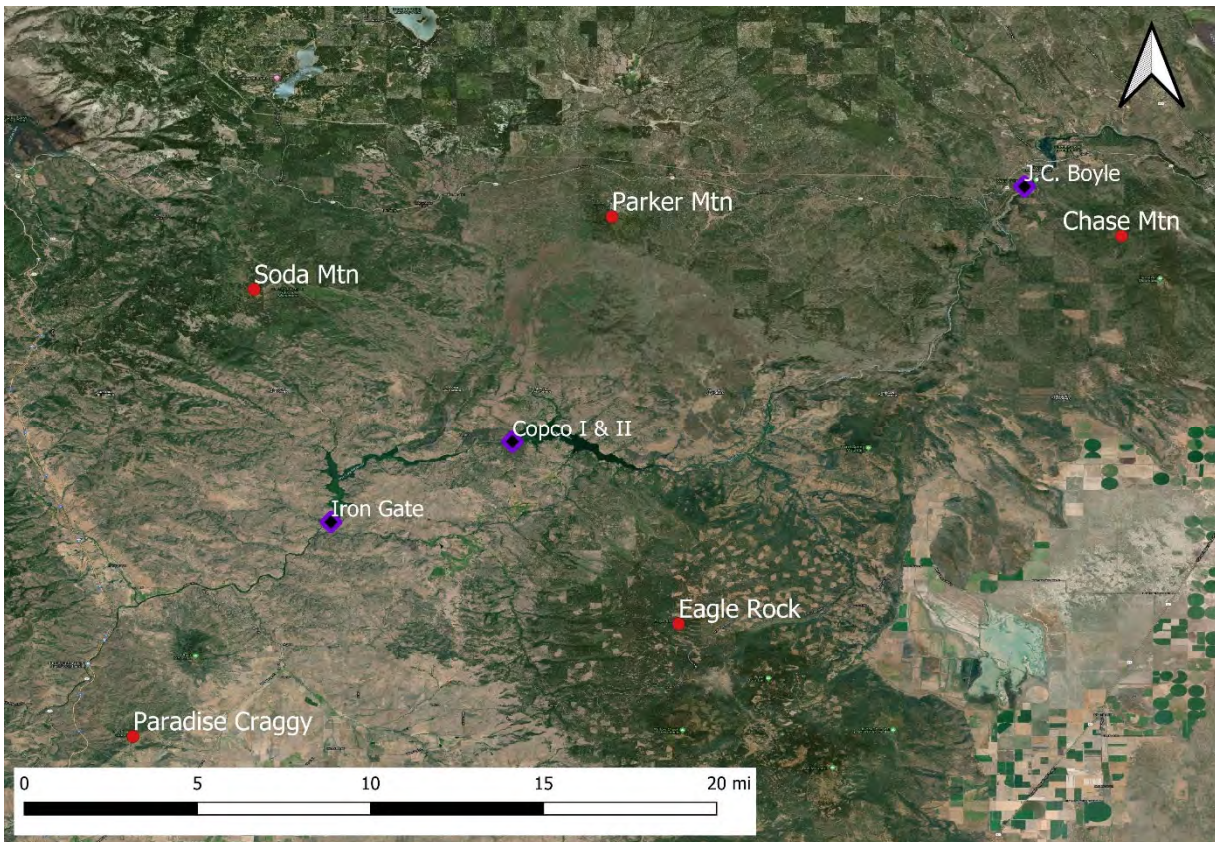


Figure 19. MDS camera locations for post-removal fire detection.

Based on the EVS camera specifications of a 12.4-mile maximum surveillance distance, a rounded value of 12 miles was applied for the radius of visibility in the viewshed analysis. This analysis includes the effect of earth curvature on visibility but does not include visibility obscuration due to haze or smoke in the lower atmosphere. The cameras were assumed to be mounted at the same height as the towers.

The viewshed analysis results illustrate coverage provided by the cameras as well as “blind spots” where no camera has visibility to the ground (Figure 20). The blue areas indicate that one of the five cameras is able to view the ground surface at that location. The green areas indicate that two of the five cameras can directly view the surface at that location; yellow indicates three cameras. There are no locations that are simultaneously visible to four or five cameras.

The results are displayed with an overlay of the ASE as this extent is understood to comprise the area of operation for CALFIRE’s aerial suppression equipment (Figure 21). With the planned removal of the four dams, this area was identified as a concern by CALFIRE as the fire risk could increase following restoration of the Klamath River to its natural watercourse.

By visual inspection of the results in Figure 21, the proposed post-removal fire detection scheme provides roughly 60-75% coverage of the protected areas in the ASE. Roughly 5-15% of this surface area is visible to multiple cameras, allowing for rapid triangulation capability in the early stages of fire growth. The proposed MDS scheme also provides detection coverage of up to 12 miles in surrounding areas of interest beyond the perimeter of the ASE. These preliminary results are positive and do not preclude the capability of the MDS to detect fires in the gray areas since the cameras could capture the smoke plume from a potential fire. However, detection and triangulation of the fire is expected to take a longer amount of time where the cameras do not have direct surface visibility.

The viewshed from Eagle Rock appears obstructed from several angles, which could be due to the assumed tower location coordinates and observer height. Additionally, the preliminary results show that there is limited direct surface visibility for about 20% of the western area of the ASE. This may be due to variations in the terrain that obstruct the line-of-sight from the cameras.

Table 2. Camera viewshed analysis inputs

| <i>MDS Camera Location</i> | <i>Radius of Visibility (miles)</i> | <i>Observer/Camera Height (ft)</i> |
|----------------------------|-------------------------------------|------------------------------------|
| Paradise Craggy Tower | 12 | 6 |
| Parker Mountain Tower | 12 | 50 |
| Chase Mountain Tower | 12 | 20 |
| Soda Mountain Tower | 12 | 10 |
| Eagle Rock Tower | 12 | 10 |

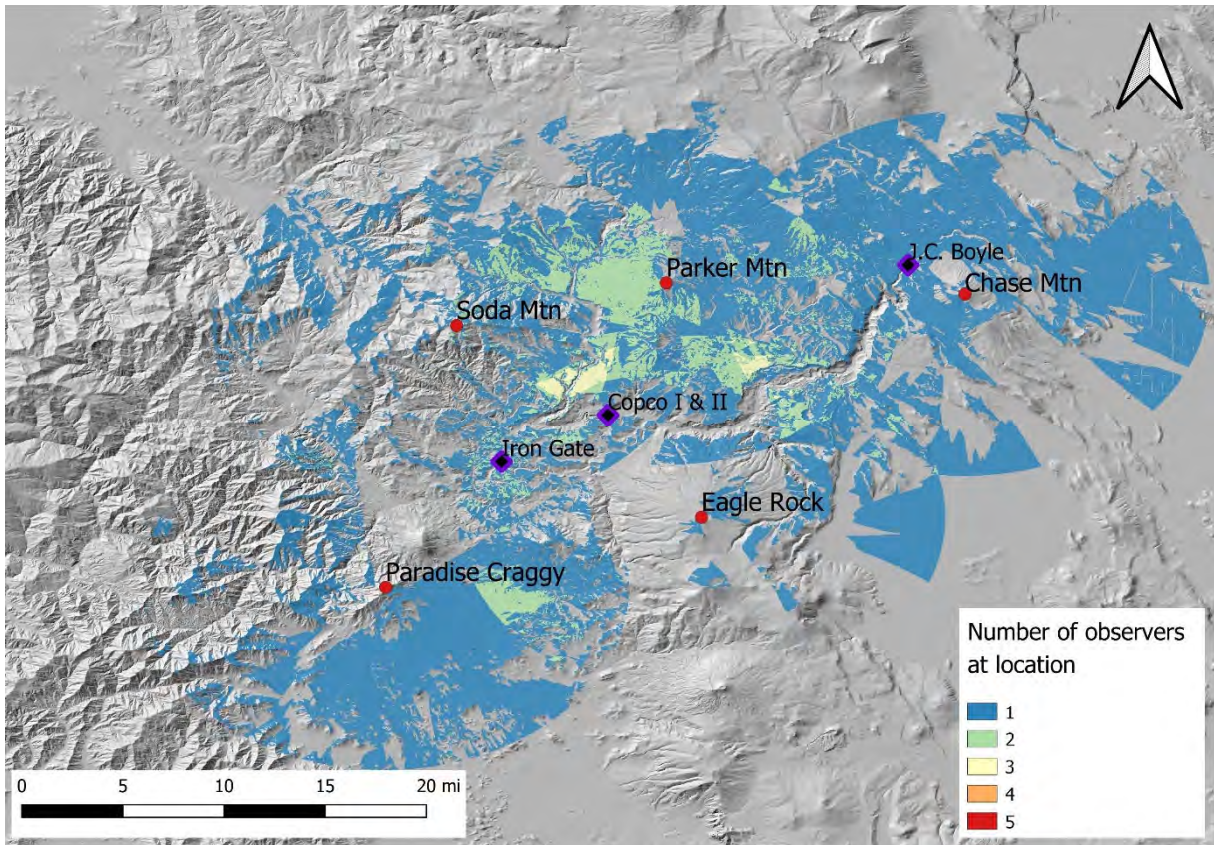


Figure 20. Post-removal fire detection viewshed analysis.

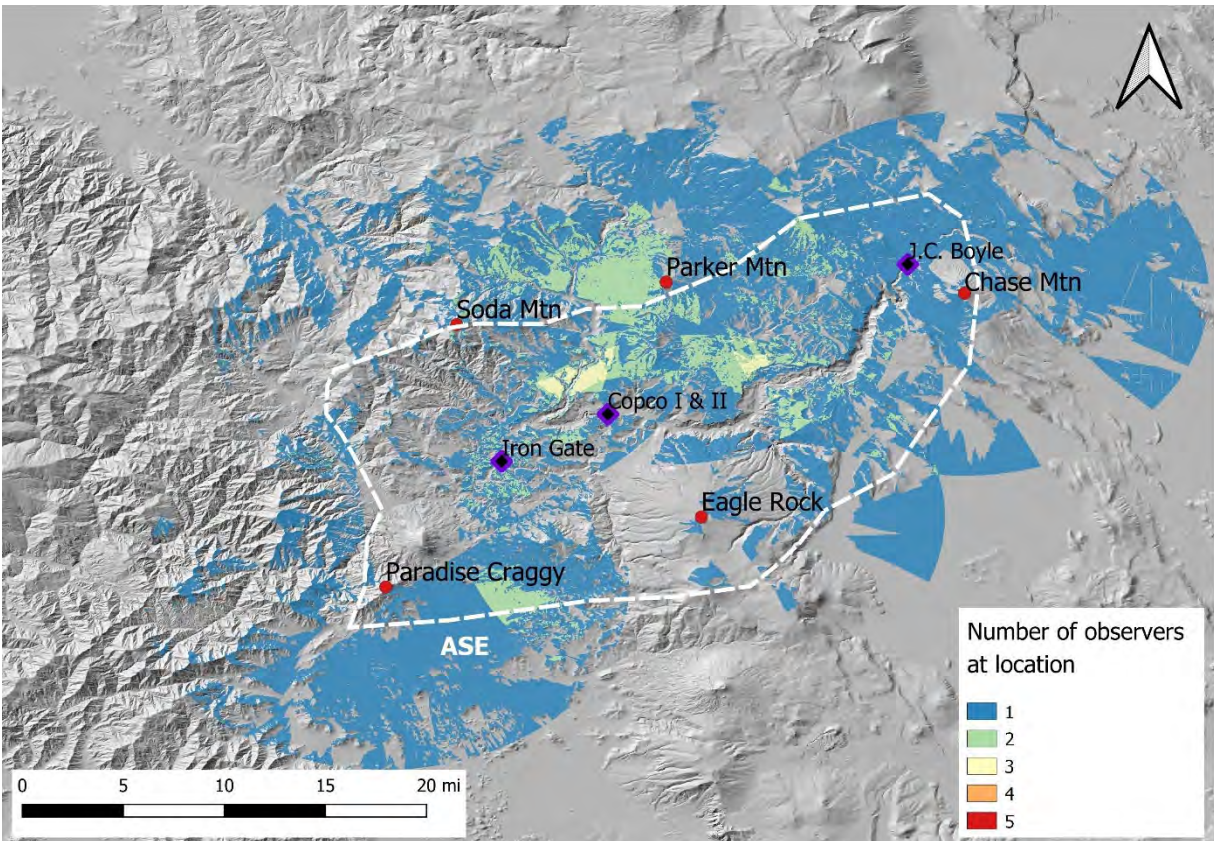


Figure 21. Post-removal fire detection camera viewshed analysis overlaid with the aerial suppression extent.

4.1.2 Alternative proposed fire detection scheme

While the preliminary results are generally positive, there is opportunity for improved robustness of the proposed MDS scheme. By installing an additional camera positioned in the northwest area of the ASE, it may be possible to eliminate some of the “blind spots”. In addition, repositioning of the Eagle Rock camera to a location with higher elevation on the mountain might provide improved coverage from Eagle Rock (Figure 22).

Several iterations of viewshed analysis were calculated from Eagle Rock by varying the camera height at its new location coordinates to determine optimal visibility. There was a fire lookout tower located in the northwest area of the Klamath Basin atop Mt. Ashland until 1959 and it is understood that there have been discussions among local fire authorities about reinstating the site for fire monitoring. Therefore, this location was chosen for siting of an additional camera for viewshed analysis of this alternate detection scheme. A viewshed analysis that incorporates these alterations is presented and discussed here (Figure 23). Camera locations that vary from those previously discussed are shown in gray. Results for improved siting of the Eagle Rock camera are presented in Table 5. The overall camera viewshed analysis for the alternate fire detection scheme with the newly added Mt. Ashland camera and the improved Eagle Rock camera location is shown in Table 5.

Table 3. Alternate MDS camera locations with additional locations shown in gray.

| <i>Tower Name/Location</i> | <i>Elevation (ft)</i> | <i>Tower Height^a (ft)</i> | <i>Longitude</i> | <i>Latitude</i> |
|----------------------------|-----------------------|--------------------------------------|--------------------------|------------------------|
| Paradise Craggy, CA | 4,890 | 6 | -122.54669 | 41.81476 |
| Parker Mountain, OR | 5,165 | 50 | -122.27865 | 42.10527 |
| Chase Mountain, OR | 6,349 | 20 | -121.99415 | 42.09461 |
| Soda Mountain, OR | 6,049 | 10 | -122.47882 | 42.06447 |
| Eagle Rock, CA | ~6,863 ^a | 10-50 ^a | ~-122.24536 ^a | ~41.88152 ^a |
| Mount Ashland, OR | 7,533 | 10 ^b | -122.71688 | 42.08073 |

^a The elevation, tower height, and location coordinates were varied to determine optimal siting [10-14].

^b A conservative tower height was assumed based on the heights of existing towers.

Table 4. Alternate camera viewshed analysis inputs.

| <i>MDS Camera Location</i> | <i>Radius of Visibility (miles)</i> | <i>Observer/Camera Height (ft)</i> |
|----------------------------|-------------------------------------|------------------------------------|
| Paradise Craggy Tower | 12 | 6 |
| Parker Mountain Tower | 12 | 50 |
| Chase Mountain Tower | 12 | 20 |
| Soda Mountain Tower | 12 | 10 |
| Eagle Rock Tower | 12 | 10-50 |
| Mount Ashland Tower | 12 | 10 |

Table 5. Improved Eagle Rock viewshed analysis siting.

| <i>Tower Name/Location</i> | <i>Elevation (ft)</i> | <i>Tower Height (ft)</i> | <i>Longitude</i> | <i>Latitude</i> |
|----------------------------|-----------------------|--------------------------|------------------|-----------------|
| Eagle Rock, CA (original) | 6,863 | 10 | -122.24536 | 41.88152 |
| Eagle Rock, CA (new) | 6,902 | 10 | -122.24175 | 41.87757 |

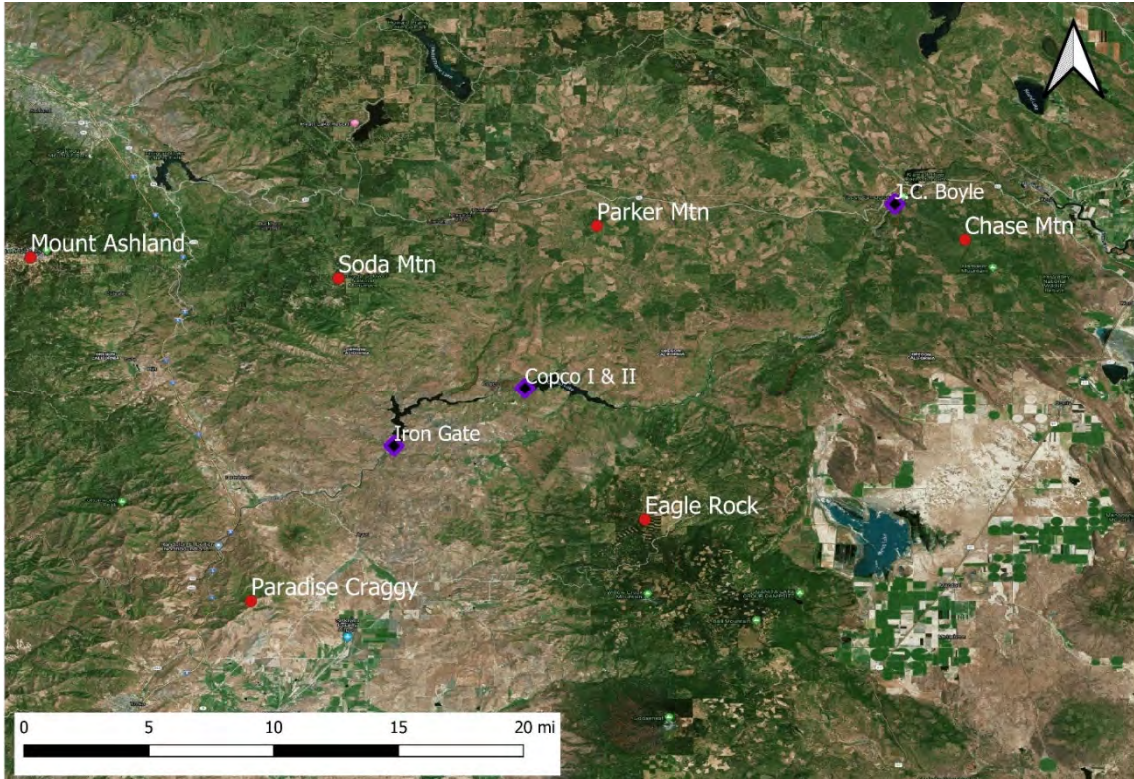


Figure 22. Proposed MDS camera locations for fire detection including Mt. Ashland.

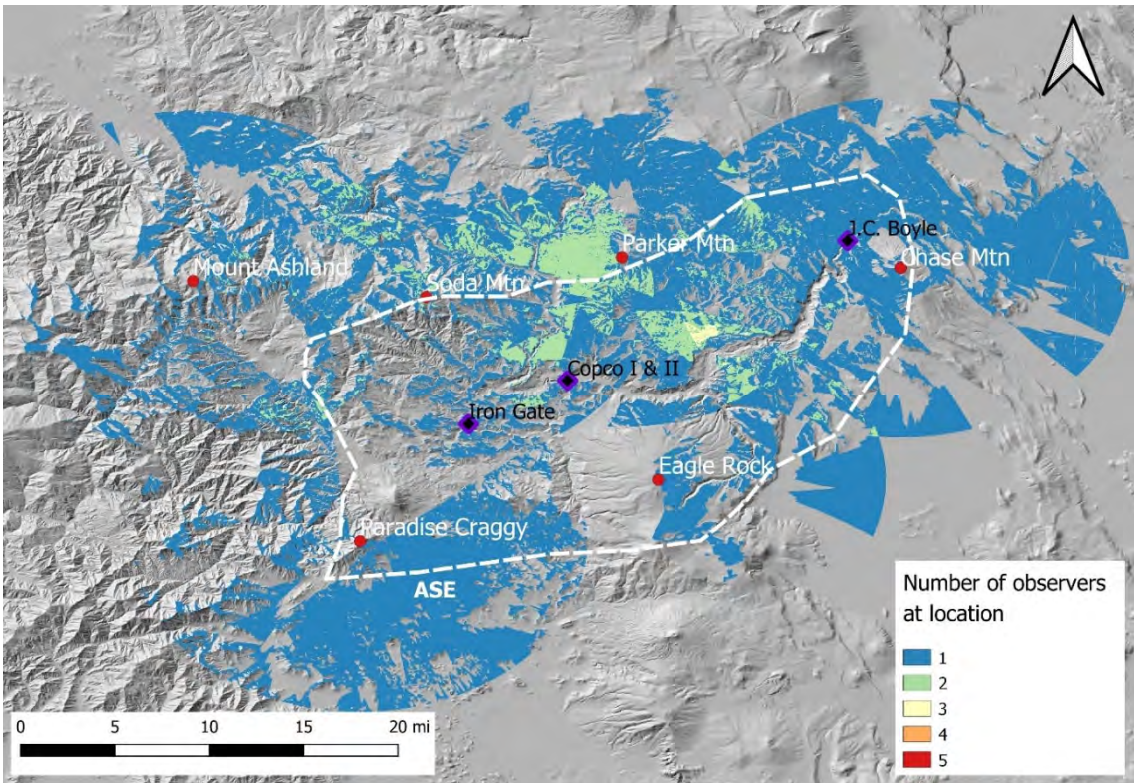


Figure 23. Results of the viewshed analysis for the alternate proposed camera scheme overlaid with the aerial suppression extent.

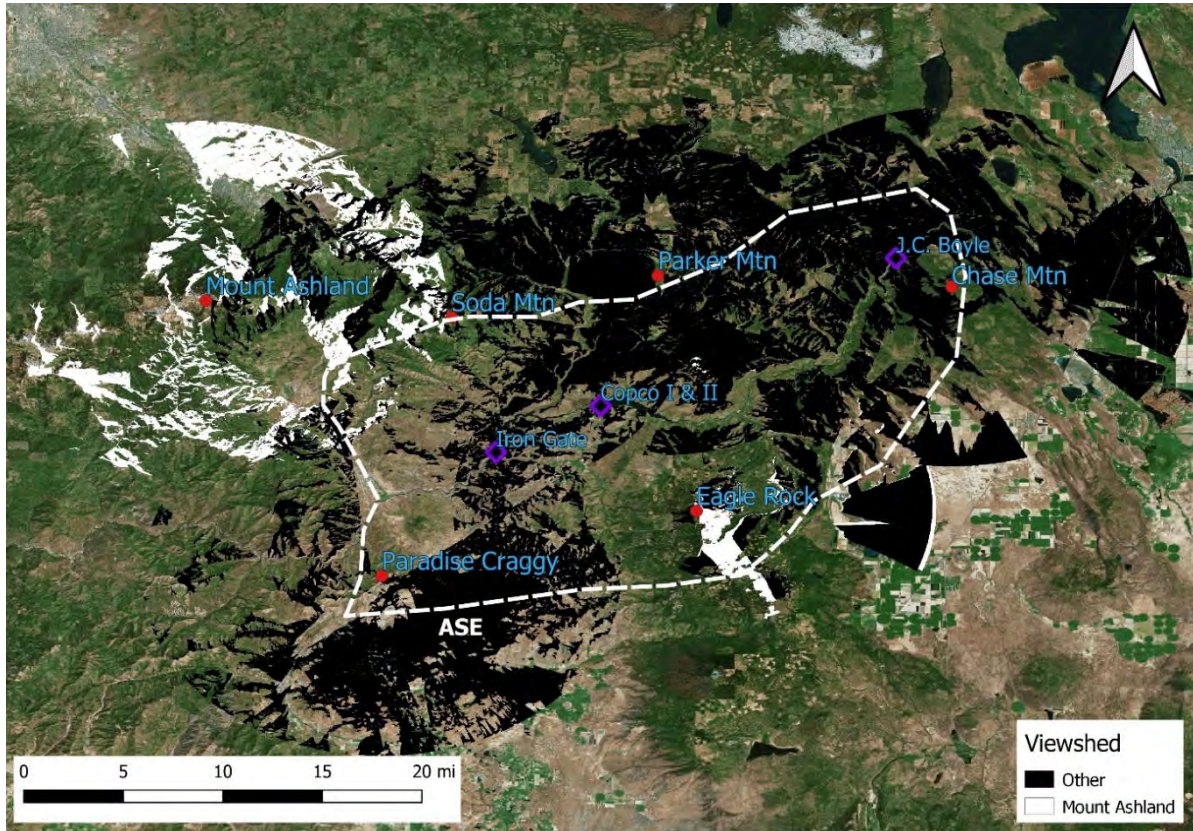
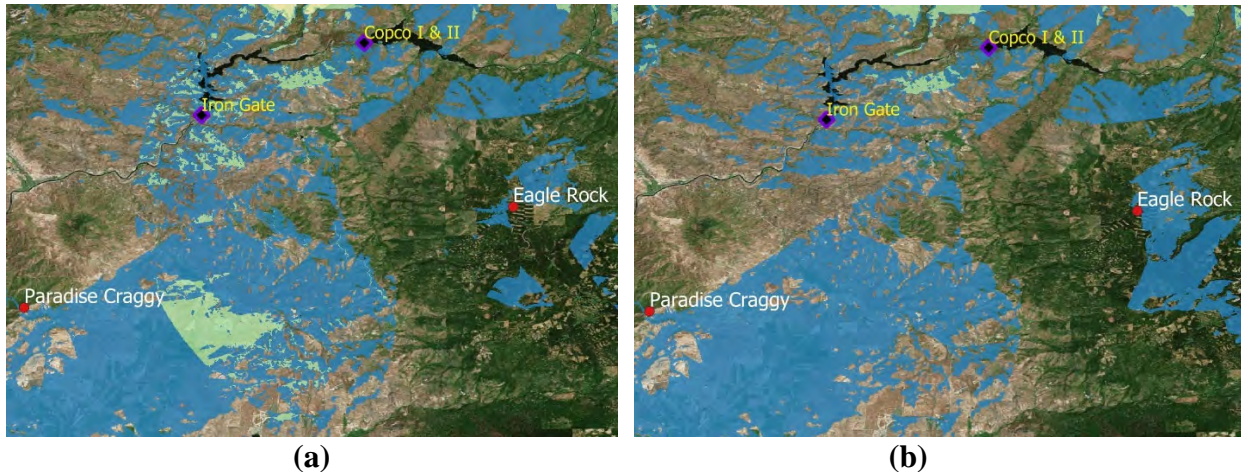


Figure 24. Post-removal viewshed analysis emphasizing Mt. Ashland contribution.

The camera viewshed analysis including Mt. Ashland shows slight improvement within the ASE and substantial improvement in surrounding areas as compared to the results from the original proposed fire detection scheme (Figure 24). The western area of the ASE still shows approximately the same amount of uncovered surface area as before, but the addition of the Mt. Ashland camera provides improved surface area coverage in the immediate vicinity of the protected area. Increasing the height of the Eagle Rock Camera in 10-foot increments from 10 feet to 50 feet above ground elevation did not have a significant effect on the viewshed. Although there was better visibility on the south side of Eagle Rock Mountain, there was a decrease in triangulated visibility between Paradise Craggy and Eagle Rock. Close comparison of the region between Paradise Craggy and Eagle Rock demonstrates this decrease in visibility as areas that were visible to two or three cameras are visible to only one (Figure 25).



**Figure 25. Viewshed of region between Paradise Craggy and Eagle Rock.
 (a) Original Eagle Rock siting. (b) Varied siting.**

4.1.3 Limitations of viewshed analysis

The limitations of a viewshed analysis, especially in the context of understanding detection effectiveness, are enumerated below.

1. The reliability of the outputs is dependent on the quality of the inputs. In this case, the analysis was reliant on the assumptions of the camera locations, heights, and radius of visibility. Due to this limitation, improvements to the quality of inputs, and thereby the quality of outputs, were made. These improvements included the manual adjustment of the camera locations based on satellite imagery of tower locations and validation of the Eagle Rock camera height through a manual sensitivity study.
2. The viewshed analysis does not account for visibility obscuration due to possible haze or smoke. Note, however, that the EVS-recommended cameras specifications include the ability to see through haze and smoke.
3. Viewshed analysis output shows camera visibility to a specified target height. In the previous discussion this target height was ground surface. For wildland fires, however, it is more likely that the camera will detect the smoke plume long before it detects actual flames (Figure 26). As part of ongoing work for this project, a refined viewshed analysis and sensitivity study will be conducted to assess detection effectiveness based on the target being a smoke plume, not the ground surface. Basing detection on the smoke plume has limitations of its own because wind and atmospheric stability influence plume height and fire growth, and therefore both would contribute to uncertainty in fire size from the smoke plume alone.



Figure 26. Smoke plume detection from a camera in the ALERTwildfire network [15].

4.1.4 Satellite-based fire detection technology

As part of the FMP detection effectiveness evaluation, the feasibility of implementing satellite-based fire detection technology developed by a commercial vendor. Using artificial intelligence (AI) and machine learning techniques, systems can produce maps in near real-time to support end-user decision-making. When the AI model detects a fire, an alert is transmitted, and the detection is then verified with “ground truth” from high-resolution (3-5 meters) imagery acquired at least once per day. Satellite-based technology provides several benefits over other detection methods, including lower false positives, higher reliability, and better precision and earlier detection.

Initial testing has shown that satellite-based fire detection may detect fire events on average approximately 10 minutes after it was first reported by civilians via phone in populated areas during the day. However, for night-time detections, particularly in areas with low population density, fires may be detected more than an hour before it is detected manually.

Due to the high cost and minimal improvement in daytime detection effectiveness relative to camera technology, this satellite-based fire detection is currently not recommended for implementation. However, several other non-commercial satellite detection systems are being evaluated for potential use as part of KRRC’s detection scheme. The non-commercial options span multiple sources including GOES-R [16] and GOES-EFD [17], in addition to work being done at universities, most notably the University of Maryland and the University of Wisconsin at Madison. The various systems emphasize different aspects of improved wildfire satellite detection.

4.1.5 Recommendations for enhanced detection effectiveness

Our recommendations for enhanced detection effectiveness are as follows:

1. As discussed in Section 4.1.3, Reax will refine the viewshed analyses to incorporate detection of smoke plumes at various heights and assess the impact this has on the degree of coverage within the analysis area and ASE. The potential correlation between smoke height and fire size at time of detection will be investigated more thoroughly.
2. The retention of a third party to assess the feasibility of camera tower construction and optimal visibility siting at the vantage of Eagle Rock is recommended. Following this assessment, the viewshed analyses can be refined to determine an optimal tower height. Camera location and height influence the viewshed results and thereby the quantification of detection effectiveness. Therefore, it is recommended that this work be carried out by the end of March so that results can be incorporated into the final analysis.

The next major step for the detection effectiveness evaluation is an analysis of the existing detection scheme to compare against the post-removal scheme. With the pre- and post-removal comparison, we can quantify the change in detection effectiveness as it relates to overall change in fire risk following Klamath River restoration efforts.

4.2 Suppression effectiveness

4.2.1 Pre-restoration

Pre-restoration suppression effectiveness establishes the benchmark for analysis of post-restoration effectiveness. The Oregon Department of Forestry (ODF) was contacted for existing fire reports and the FOD [1] was used to spatially locate past fire occurrences. The stated CALFIRE suppression acreage goal for all fires is 10 acres. ODF has a suppression goal of keeping fires as small as possible.

4.2.2 Post-restoration

The effectiveness of post-restoration suppression will be determined in the Monte-Carlo fire spread analysis presented in Section 5.0. Randomly selected fire ignitions will be analyzed for fire growth in hourly increments over a 12-hour period and the available suppression resources in the KRRC area will be assessed against these modelled fires. Additional suppression resources will be added to the existing inventory to determine if additional resources improve efficiency. This may include engines and hand crews, water tenders, and water source locations in addition to what is already in place over the KRRC area.

4.2.3 Quantification methodology

Statistically, approximately 90 percent of wildland fires in the US are suppressed in the first 48 hours. The other 10 percent which are not successfully suppressed initially due to an extreme but rare combination of fuel conditions and fire weather become campaign fires such as the Klamathon Fire. The federal government has studied this in depth and determined that it is unrealistic to keep increasing the suppression capacity nationally beyond a certain budgetary level. In other words, no matter how many resources are mobilized on a fire, fires occurring during weather events above

the 90th percentile may not be successfully suppressed in the first 48 hours. Typically, the Federal budget is at or near this 90th percentile level of suppression success on a local level.

The few fires that escape initial attack (IA), like the Klamathon Fire, are the ones that burn the most area. Success in IA is dependent on several factors including weather conditions, fire detection time, fire service arrival time, fire spread rates, fire line production rate, and budget constraints. Causes of fire, where known, can be divided into human-caused and lightning-caused. Human-caused fires tend to occur near roads and trails and average significantly lower response times than lightning-caused ignitions. The distinction between the two predominant fire causes is important because it inherently affects many of the factors influencing IA success.

In a study by Rodrigues *et al.* [18], the probability of IA success was calculated as a combination of the time to detection, travel time, fire spread potential, and available resources. Time to detection was based on viewshed analyses from roads and towns. Because the smoke plume is more likely to be seen than the fire itself, a 300 m offset height was added to the Digital Elevation Model (DEM). The greater the number of locations from which a particular pixel could be seen, the more rapid the detection time. Arrival time after dispatch was assessed with variations allowing for paved roads, unpaved roads, and walking trails. Accessibility via paved roads was calculated using the Euclidean distance from the fire stations. Unpaved roads and trails were evaluated using a cost-distance function and the difficulty of walking was estimated using terrain slope from the DEM. The objective of the cost-distance function is to determine the least costly path of travel in terms of time. Aerial resources were modeled using the Euclidean distance to heliports. Resources available for IA efforts are capable of handling most fires under normal circumstances. An exception to this is when multiple fires occur which forces incident command to evaluate where the finite number of resources may be most effective in light of the potential assets at risk. In the study, this was modelled by calculating the number of fires burning simultaneously. Fire spread potential is largely dependent on meteorology, fuel types, and topography therefore the study used gridded weather data corresponding to the date of historical escaped fires, five fuel types from land cover maps, and the DEM.

Results from this study showed the response time from initial detection to first-on-scene to be the most critical factor in success of IA. Stemming from this result, the distance to fire stations and heliports were the next most significant factors. Visibility from road networks followed these contributions in importance. Accessibility on foot was the next contributing factor. Dynamic factors such as weather and available resources constituted the smallest influence. It is important to note that although these dynamic factors appear comparatively insignificant, they are linked to extreme fire events and therefore are crucial for identifying hazardous conditions.

Another study by Reimer *et al.* [19] investigated suppression effectiveness by pairing burn probability and containment probability calculations. Containment probability calculations were based on fire intensity, spread rate, and response time. Success in containment is highly correlated with fire size and intensity at the time of IA and was predicted using these factors. Stochastic ignitions and weather were used for fire growth modeling, with the final result being an estimation of burn probability. Two simulations of this fire growth modeling were completed, one with suppression and one without. Records of ignitions over a 90-year period were analyzed to identify spatiotemporal patterns. Human-caused ignitions clustered around features like roads and

campgrounds while lightning caused ignitions were weather and topography driven. Response times to human-caused fires on average are lower because of proximity to roads and access routes. Because suppression activities during moderate weather prevent ignitions from lasting until fire weather improves, this study assumed that if a fire escapes initial attack suppression activities would not significantly reduce spread rates.

This study did not account for crew size, detection networks, proximity to water, or variations in response time other than cause. Even with these limitations, the study indicates that response time is again a key component in determining IA success. A more insidious component that may prove difficult to quantify is the increased risk in following years from suppression. One of the tributary conclusions addressed this concern, suggesting that permitting certain fires under moderate weather can reduce hazard in subsequent years while keeping short-term risk low.

A methodology similar to Reimer *et al.* [19] will be used to quantify suppression effectiveness within the analysis area. Spatial burn probabilities generated in the Monte-Carlo fire spread analysis will be used and combined with containment probability calculations. These containment probability calculations will be unique to each suppression asset which will allow different combinations of assets to be analyzed. Containment calculations will be based on fire intensity, rate of spread, and response time to each fire.

4.2.4 *Conclusions and next steps*

The amount and accessibility of water for suppression will not be reduced by the removal of the reservoirs created by the dams (Figure 27). As the FMP illustrates, the planned river access points, boat launches, and fishing access points will provide key drafting points for engines and water tenders. Also, the six planned dry hydrants and the six existing pressurized hydrants will provide viable water access points for ground-based equipment and to support aerial water delivery.

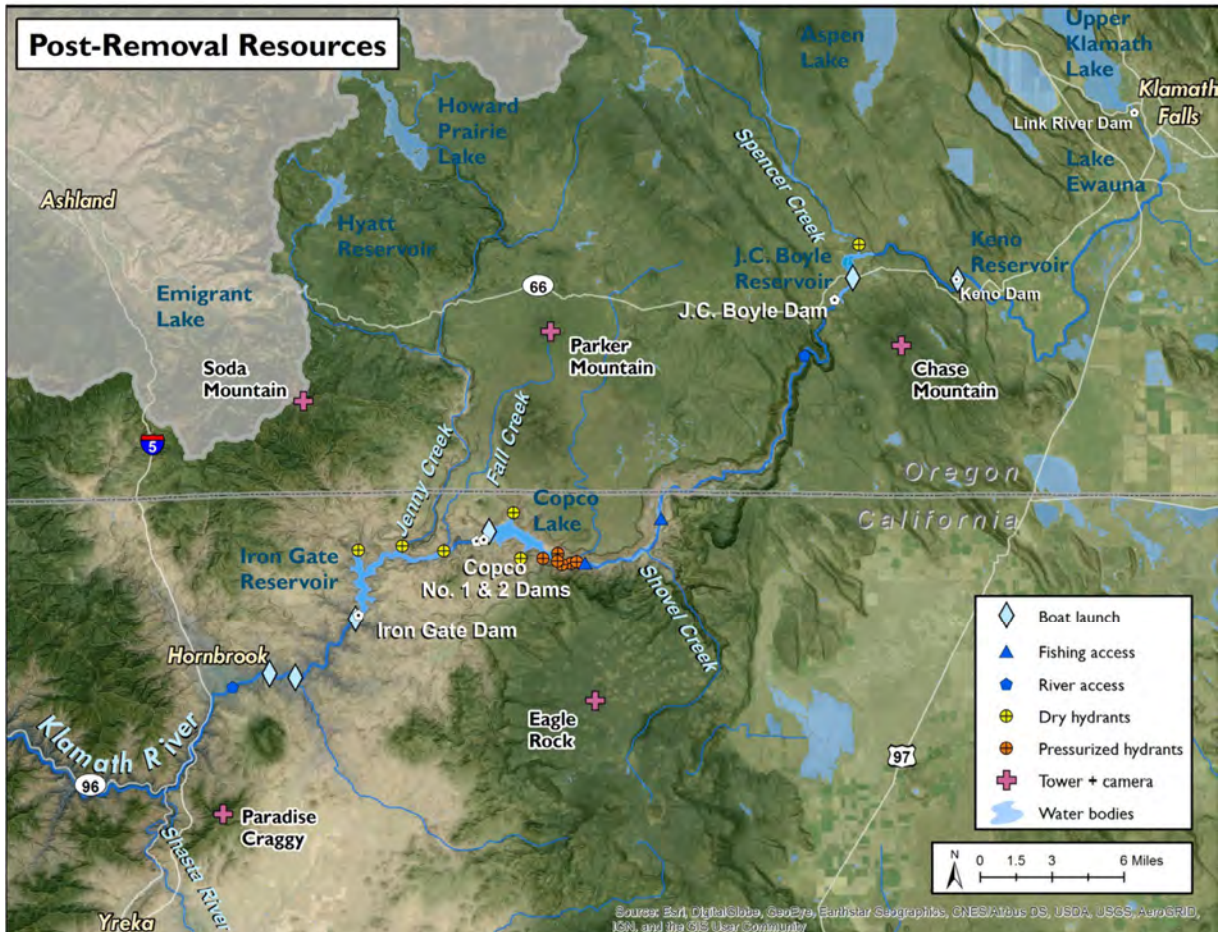


Figure 27. Post-removal management resources provided as part of the long-term FMP [6].

There are currently 96 inventoried river pools of varying risk classes for helicopter bucket work and another predicted 41 helicopter bucket sites of varying risk categories in the current reservoir pool areas (Figure 28). With around 137 pools for helicopter bucket use and a minimum of 18 other river access sites available for drafting, the ability to use water for fire suppression will not be impacted. The convenience of using some sites, such as reservoirs, may be impacted but the overall amount of water available should not be affected by dam removal. The minimum river discharge of 900 ft³/s will be sufficient to maintain a good water supply for suppression forces.

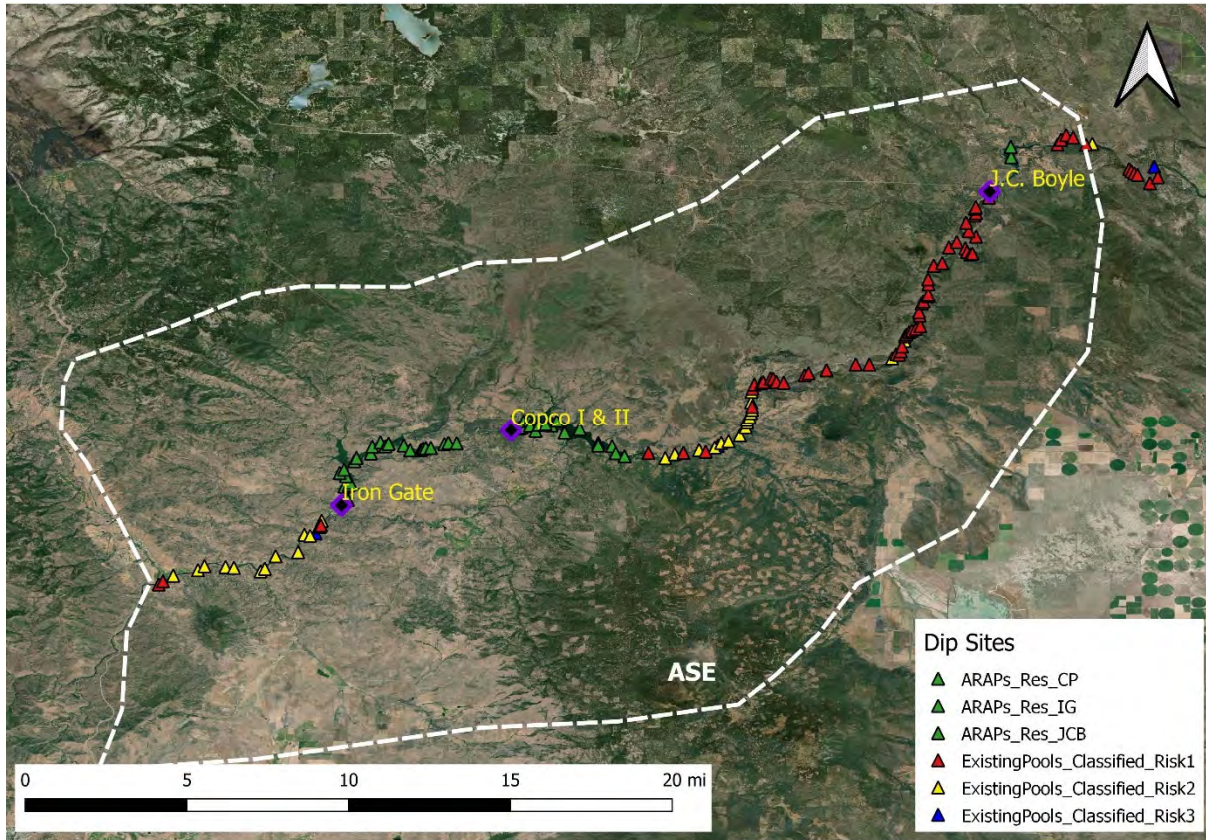


Figure 28. Pre- and Post-restoration dip sites.

Portable rigid tanks (fold-a-tanks) could be staged in pre-determined sites along both sides of the river corridor to supplement aerial and ground-based water supply for engines, helicopters, etc. Fold-a-tanks up to 20,000 gallons in size could be stored, erected, and filled rapidly for initial attack activities at these selected sites or moved and set up at other sites (Figure 29). Portable soft-sided water tanks of up to 360 gallons could be staged at these same sites to be air-lifted by helicopter to remote fire sites needing additional water supply (Figure 30). Additional engines or water tenders will be analyzed as well to see if any gain in effectiveness can be achieved with more of these resources.



Figure 29. Rigid tank model shown with helicopter snorkel.



Figure 30. Soft-sided tank model being airlifted.

5.0 MONTE-CARLO FIRE SPREAD MODELING

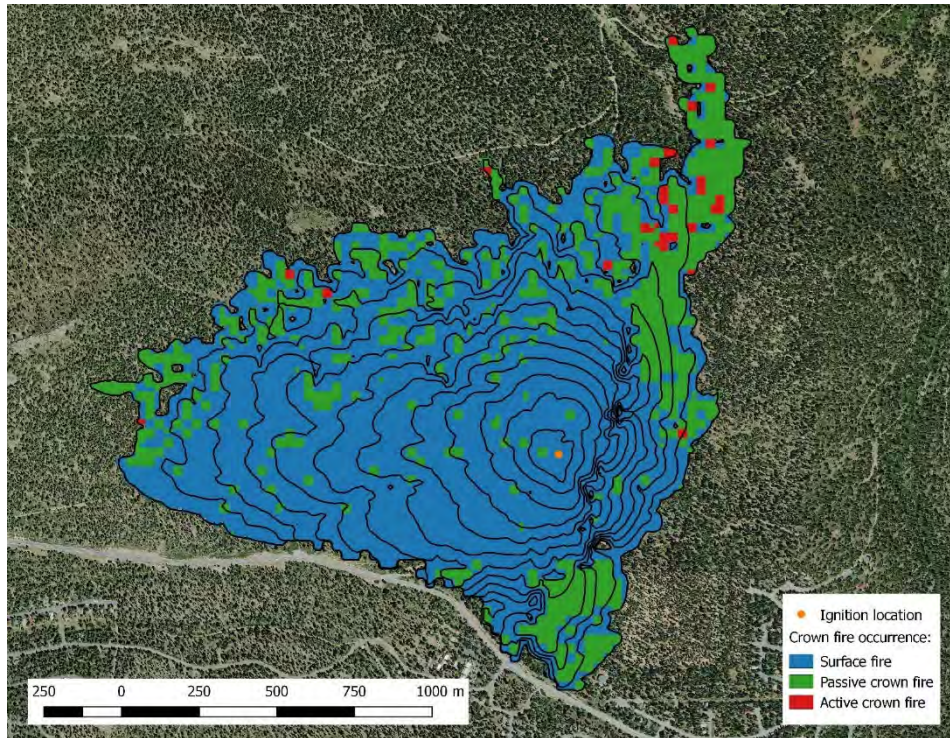
Wildland fire hazard/risk assessment using fire behavior modeling has recently seen increased usage due in part to more powerful computational resources, improved fire models, and readily available geospatial input data. Keane *et al.* [20] highlighted the potential for Monte-Carlo analysis to be used for wildland fire risk quantification, stating “Andrews (2007) FSPRO approach in which maps of fire intensity distributions are computed from thousands of FARSITE [21] runs is perhaps the most significant step towards fine scale risk mapping.” One advantage of such an approach is that fire shadows, islands, and related effects can be captured. Monte-Carlo simulations where fire spread is modeled from tens of thousands of separate ignition locations under a range of weather conditions is one of the most promising tools for quantitative wildland fire risk/hazard assessment.

Furthermore, this same basic approach has already been successfully applied in Victoria, Australia, to quantify fire risk associated with overhead electrical utility ignited fires [22-26] and was also applied recently in California [27-34] to map hazard from powerline fires. For this reason, the basic methodology applied in Australia and California to map utility-associated fire risk is used as the basis in the current project to map change in fire risk associated with the removal of the four dams.

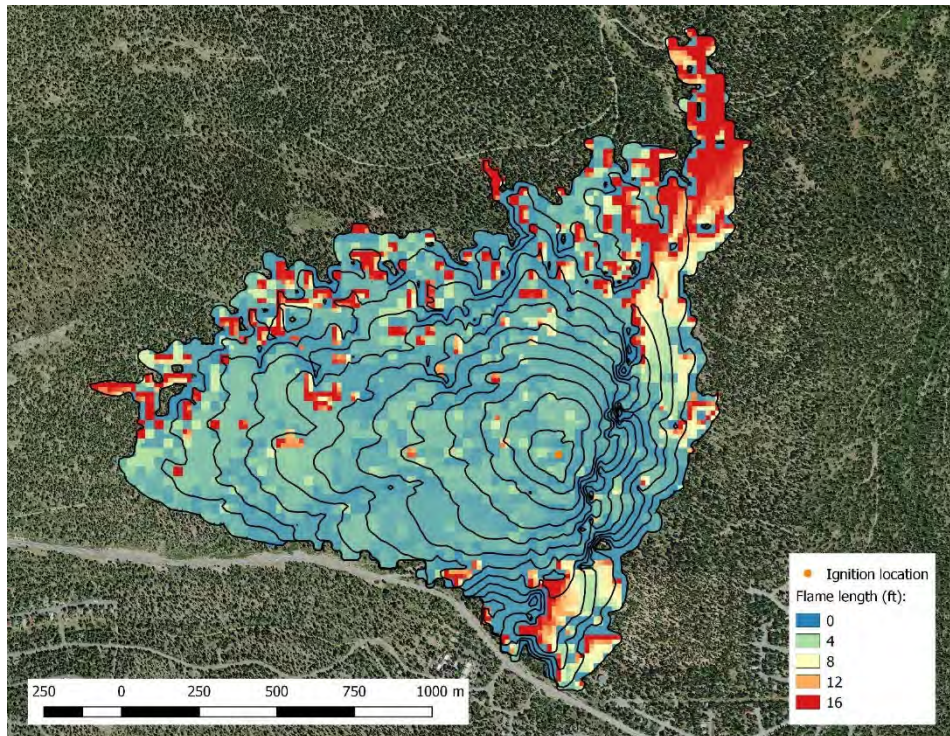
5.1 Monte-Carlo fire spread model: ELMFIRE

The open source software ELMFIRE [32-33] (Eulerian Level Set Model for Fire Spread) is used here to quantify wildland fire hazard via Monte-Carlo analysis. ELMFIRE’s computational engine is similar to other two-dimensional fire simulators such as FARSITE [21] or PHOENIX RapidFire [22-26] in that it calculates surface fire spread rate using the Rothermel surface spread model [36, 37], assumes that each point along the fire front behaves as an independent elliptical wavelet [38] with length to breadth ratio determined semi-empirically [21, 39], and simulates transition from surface to crown fire using the Van Wagner criterion [40] (with passive/active crown fire spread rates calculated from Cruz *et al.* [41]). ELMFIRE tracks the fire front using a narrow band level set method [42], a numerical technique for tracking curved surfaces on a regular grid.

To demonstrate how ELMFIRE simulates fire spread, Figure 31 shows 24-hours of fire progression from an individual ignition site. The black contour lines in Figure 31 a represent fire front position at 2-hour intervals. Figure 31a also shows which parts of the burned area experienced surface fire (blue), passive crown fire (green), or active crown fire (red). Figure 31b similarly shows fire perimeter contours and flame length variation within the fire perimeter. Flame length is highest in areas that burn as heading fires or that experience crown fire, and lowest in areas that burn as a flanking or backing fire or as a surface fire. In this example, fire area after 24 hours of spread is approximately 560 acres.



(a)



(b)

Figure 31. Sample ELMFIRE fire spread simulation for individual fire ignition. (a) Fire type (surface fire, passive crown fire, or active crown fire). (b) Flame length.

5.2 Fuels

Fuel and topography layers in the analysis area were obtained from the LANDFIRE Remap (LANDFIRE 2.0.0) database [43-44] at a resolution of 30 m. Topography layers include elevation, slope, and aspect. Fuel layers include surface fuel model (in the Scott and Burgan 40 system [45]), canopy height, canopy cover, canopy base height, and canopy bulk density.

5.2.1 Pre-restoration

Existing vegetation rasters from LANDFIRE Remap were assessed for the types of vegetation expected in the areas surrounding the reservoirs (Figure 32). The numerical values of the fuel types do not provide insight into fire behavior but the descriptions provided by Scott and Burgan [45] do. The major fuel types found around the Iron Gate and Copco reservoirs are described as follows:

- 91 (Urban/Developed) – consists of urban and suburban development that does not support wildland fire spread.
- 98 (Open Water) – land covered by open bodies of water such as lakes and rivers.
- 99 (Bare Ground) – land devoid of sufficient fuel to support wildland fire spread such as deserts, rock outcroppings, and beaches.
- 102 (Low Load, Dry Climate Grass) – primary carrier of fire is semi-continuous grass.
- 121 (Low Load, Dry Climate Grass-Shrub) – primary carrier of fire is grasses and small (1 ft.) shrubs together with moderate fire spread rate.
- 122 (Moderate Load, Dry Climate Grass-Shrub) – primary carrier of fire is grass and medium (1-3 ft.) shrubs together with high fire spread rate.
- 165 (Very High Load, Dry Climate Timber-Shrub) – primary carrier is heavy forest litter with a small tree or shrub understory with moderate fire spread rate.
- 186 (Moderate Load Broadleaf Litter) – primary carrier is moderate load broadleaf litter with moderate fire spread rate.

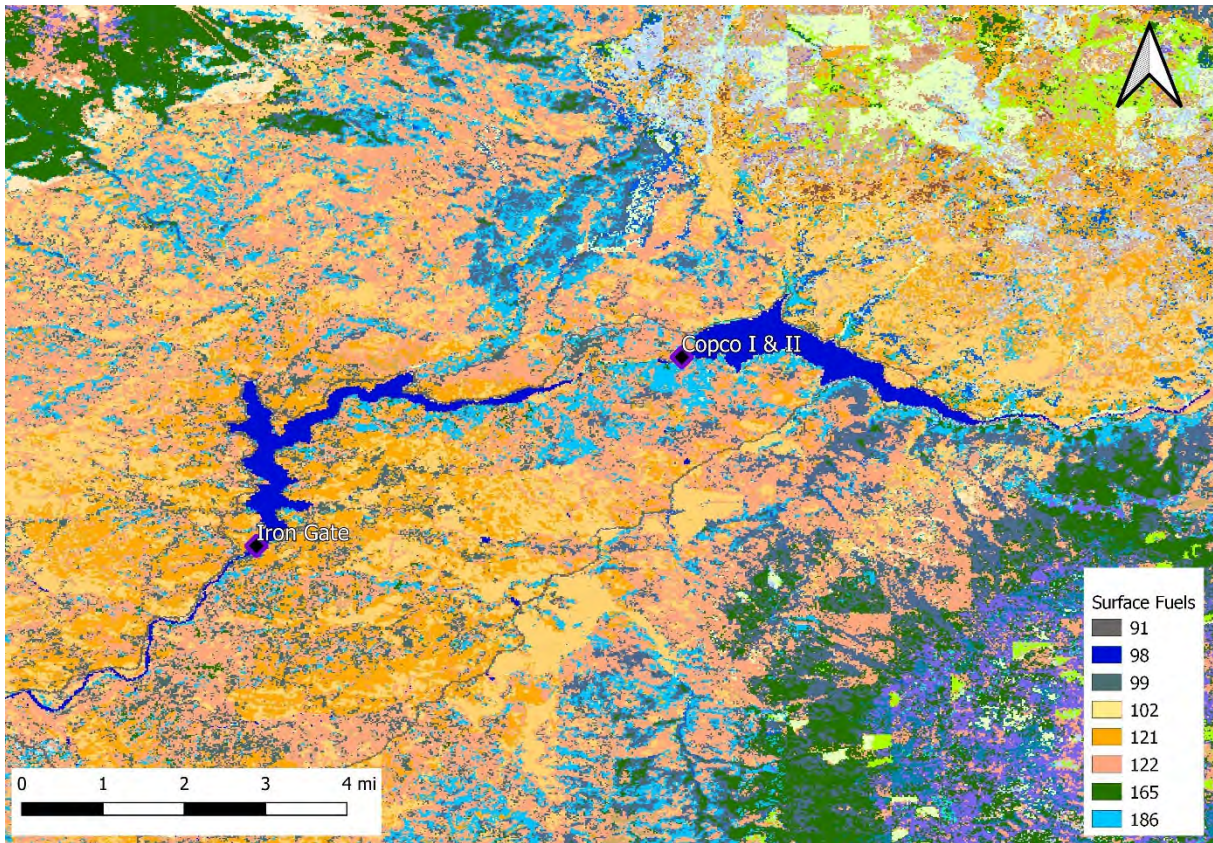


Figure 32. Iron Gate and Copco surface fuel pre-restoration

5.2.2 Post-restoration

Vegetation re-growth after dam removal was estimated using historical imagery and existing vegetation types surrounding the areas to be reclaimed. Existing vegetation typically is a good surrogate for expected re-growth in an area of similar soils, *etc.* The Fuels Classification and Characterization System (FCCS) [46] was utilized as well as LANDFIRE data [43-44] for the analysis area (Figure 33, Figure 34). The LANDFIRE vegetation type was compared to the FCCS existing vegetation to verify the potential vegetation for the site.

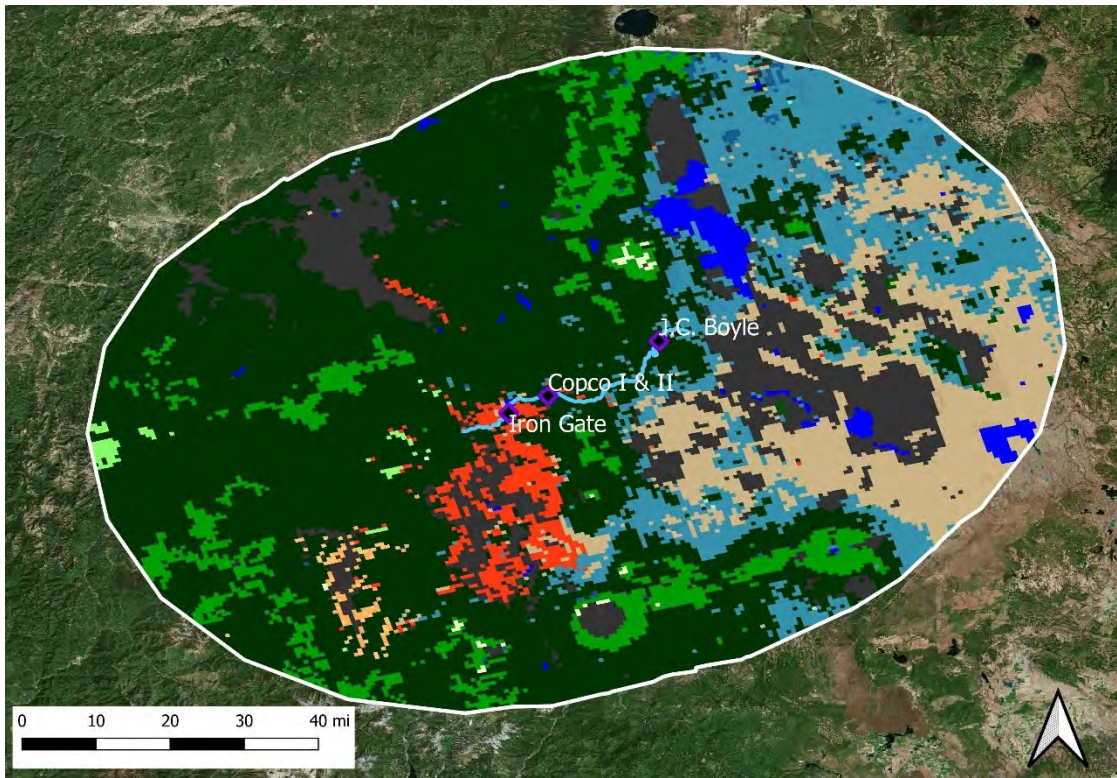


Figure 33. FCCS existing vegetation types.

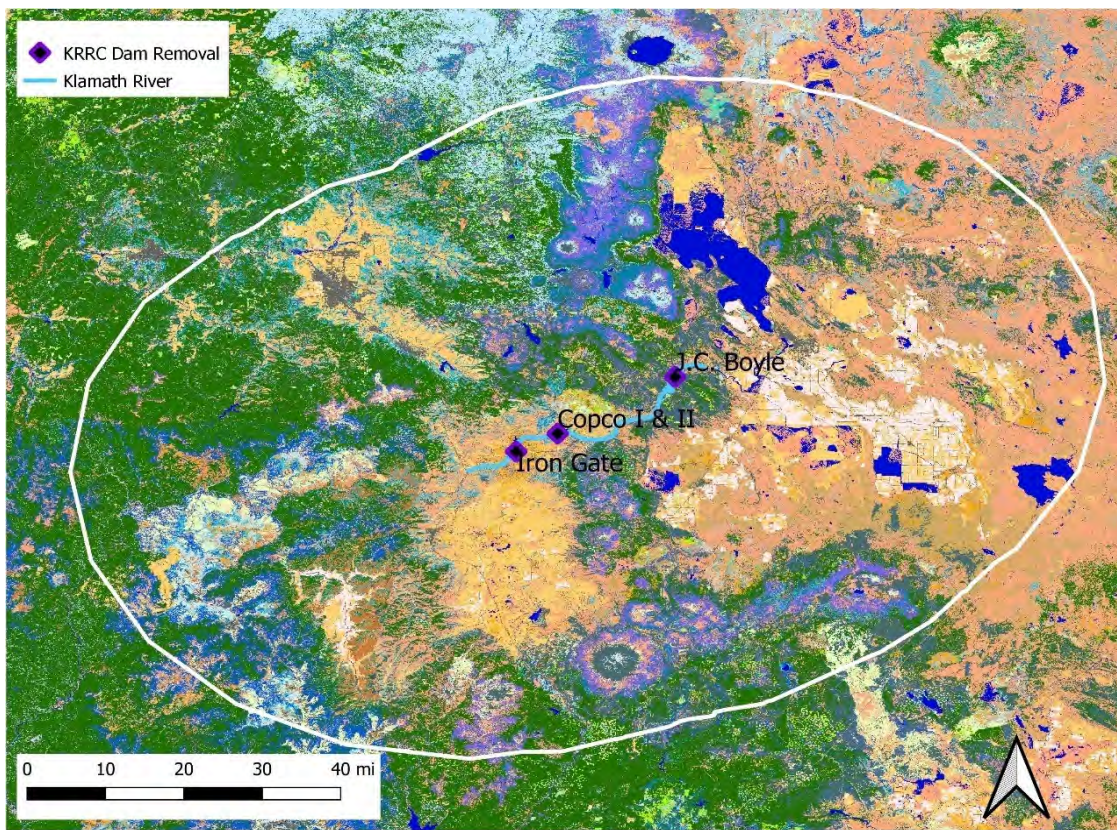


Figure 34. LANDFIRE 2.0.0 (Remap) existing vegetation types.

Initial re-growth is assumed to be in the grass-forb stage for up to the first ten years after the dams are removed. An example of post-restoration fuels is shown in Figure 35 with reclaimed land as fuel model 101 (short grass).

The second decade in grass dominated areas will remain grass. In shrub-chaparral areas the second ten-year increment (10-20 years) will move into a shrub-grass and in the third ten-year increment the vegetation will return to a shrub-chaparral vegetation type, such as the Chamise chaparral shrubland adjacent to the Iron Gate Dam area. Grass-forb and chaparral-shrub vegetation types have a relatively short developmental cycle and are considered mature within 30 years of re-establishment.

After the first ten-year increment forested areas will move into a shrub-grass type for the next ten years, followed by a timber-grass type as reforestation grows above the initial grass-shrub stages. These stages will be followed by a timber type which will mimic the existing timber type in the immediate area, such as the Jeffery pine, Ponderosa pine, and Douglas-fir forests around the Copco I and II site.

Once the revegetated timber areas reach the fifth ten-year increment it is assumed that they will be similar in type to the surrounding areas of vegetation but will not be in a similar age class or stage of development.

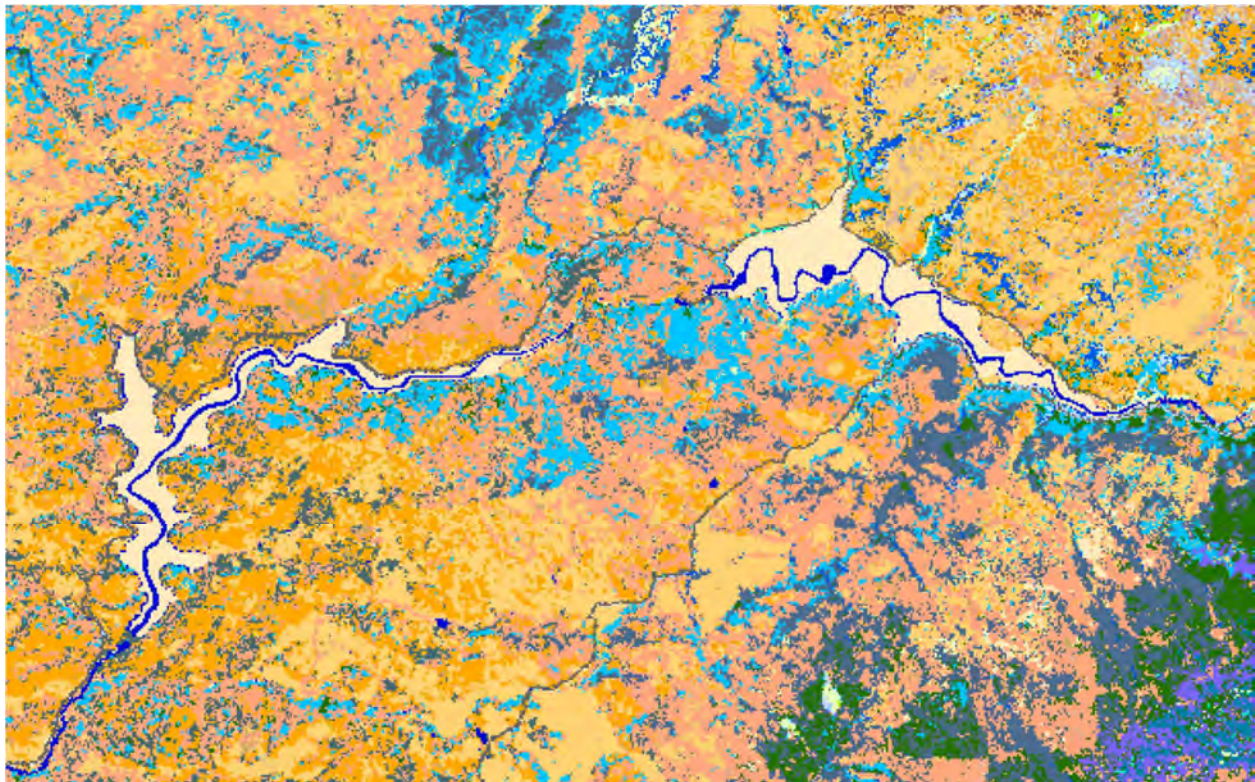


Figure 35. Iron Gate and Copco surface fuels post-restoration.

5.3 Fire weather

The general approach to developing wind and weather inputs involves using the North American Regional Reanalysis (NARR) dataset [47] in conjunction with a fire weather filter to identify days of historic weather significance. The Weather Research and Forecasting (WRF) model is then used to generate wind and weather fields only for those days identified as being significant from a fire weather perspective.

The NARR dataset is maintained by the National Centers for Environmental Prediction, the National Weather Service, and the National Oceanic and Atmospheric Administration. It is a gridded meteorological dataset that provides a “snapshot” of the atmosphere every 3 hours at approximately 32 km resolution. Being a reanalysis, NARR is a hybrid of weather modeling and meteorological observations (surface observations of temperature, relative humidity, wind speed/direction, and precipitation, weather balloon observations of wind speed/direction and atmospheric, sea surface temperatures from buoys, satellite imagery for cloud cover and precipitable water, *etc.*). Ingested data include not only surface (meaning near ground level) quantities but also upper atmosphere quantities as well. The NARR dataset is available from 1979 when modern satellites first became available to current day, with a lag of a few weeks.

Although NARR’s 32 km resolution is too coarse to be useful for fire spread modeling purposes, it can be used to identify historical fire weather days to be recreated at higher resolution using WRF. The basic idea is to determine dates for each 32 km by 32 km NARR pixel in the analysis area where the most severe fire weather conditions have occurred between 1979 and 2018. The primary advantage of identifying historical fire weather events using reanalysis data, instead of surface (weather station) observations, is that the NARR dataset is both spatially and temporally uniform whereas point observations are not.

5.3.1 Methodology

The first step to identify historical fire weather days is selection of a single criterion that can be used to identify the most severe fire weather conditions in the NARR dataset. While there are many possibilities, a modification to the Fosberg Fire Weather Index (FFWI) [48] was selected. FFWI combines temperature, relative humidity, and wind speed into a single index ranging from 0 to 100, with 100 corresponding to a wind speed of 30 mph and fine fuel moisture content of 0%. The FFWI formula is presented as Equation 1:

$$\text{FFWI} = \eta \sqrt{1 + U^2} \quad (1)$$

where U is the 20-ft wind speed in miles per hour and η is a function of equilibrium moisture content, M_{eq} :

$$\eta = 1 - 2 \left(\frac{M_{eq}}{30} \right) + 1.5 \left(\frac{M_{eq}}{30} \right)^2 - 0.5 \left(\frac{M_{eq}}{30} \right)^3 \quad (2)$$

In Equation 2, M_{eq} is calculated as [49, 50]:

$$M_{eq} = \begin{cases} 0.03 + 0.28 \times RH - 0.00058 \times RH \times T & \text{for } RH < 10\% \\ 2.23 + 0.16 \times RH - 0.0148 \times T & \text{for } 10 \leq RH < 50\% \\ 21.1 - 0.4944 \times RH + 0.00557 \times RH^2 - 0.00035 \times RH \times T & \text{for } RH \geq 50\% \end{cases} \quad (3)$$

where RH is relative humidity in percent and T is temperature in °F.

FFWI is very sensitive to wind speed, and less sensitive to relative humidity and temperature. For example, FFWI is 80 for a wind speed of 50 mph and an equilibrium moisture content of 10%, but only 73 for a wind speed of 25 mph and an equilibrium moisture content of 2%. Ignition of a wildland fire and growth to threatening scales may be more likely under the latter conditions, but spread rates for an already established wildland fire could be higher under the former conditions.

It has been found that using a Fosberg Fire Weather Index (FFWI) could result in “off season” (generally, during the winter, *i.e.* after significant rains) days being falsely identified as fire weather days. To avoid these problems, a Modified Fosberg Fire Weather Index (MFFWI) is used in this work to identify wind events that occur simultaneously with low relative humidities and high temperatures. MFFWI is defined as follows:

$$MFFWI = FFWI \times \frac{P_{ign}}{100} \quad (4)$$

where P_{ign} is Schroeder’s ember ignition probability [51] as given in Table 6 as a function of fuel temperature and fine fuel moisture content. The data were originally published [51] with temperatures in degrees Fahrenheit and this convention is retained here. It is seen that the ember ignition probability is strongly sensitive to moisture content, and less sensitive to temperature.

Table 6. Ignition probability by woody embers/firebrands as tabulated by Schroeder [51].

| Fuel Temp (F) | Fine Fuel Moisture Content (%) | | | | | | | | | | | | | | |
|------------------|--------------------------------|-----|-----|-----|-----|-----|-----|-----|------|-------|-------|-------|-------|-------|-----|
| | 1.5 | 2.0 | 2.5 | 3.0 | 4.0 | 5.0 | 6.0 | 7-8 | 9-10 | 11-12 | 13-16 | 17-20 | 21-25 | 26-30 | >30 |
| 30-39 | 87 | 80 | 74 | 69 | 59 | 51 | 43 | 34 | 25 | 17 | 10 | 4 | 1 | 0 | 0 |
| 40-49 | 89 | 83 | 77 | 71 | 61 | 53 | 45 | 36 | 26 | 18 | 11 | 5 | 1 | 0 | 0 |
| 50-59 | 92 | 85 | 79 | 73 | 63 | 54 | 47 | 37 | 27 | 20 | 11 | 5 | 2 | 0 | 0 |
| 60-69 | 94 | 88 | 81 | 76 | 65 | 56 | 49 | 39 | 29 | 21 | 12 | 6 | 2 | 0 | 0 |
| 70-79 | 97 | 90 | 84 | 78 | 68 | 59 | 51 | 41 | 30 | 22 | 13 | 6 | 2 | 0 | 0 |
| 80-89 | 100 | 93 | 87 | 81 | 70 | 61 | 53 | 42 | 31 | 23 | 14 | 7 | 2 | 1 | 0 |
| 90-99 | 100 | 96 | 90 | 84 | 73 | 63 | 55 | 44 | 33 | 24 | 15 | 7 | 3 | 1 | 0 |
| 100-109 | 100 | 99 | 93 | 86 | 75 | 66 | 57 | 46 | 35 | 26 | 16 | 8 | 3 | 1 | 0 |
| 110-119 | 100 | 100 | 96 | 89 | 78 | 68 | 59 | 48 | 36 | 27 | 17 | 9 | 3 | 1 | 0 |
| 120-129 | 100 | 100 | 99 | 93 | 81 | 71 | 62 | 51 | 38 | 29 | 18 | 9 | 4 | 1 | 0 |
| 130-139 | 100 | 100 | 100 | 96 | 84 | 74 | 65 | 53 | 40 | 30 | 20 | 10 | 4 | 1 | 0 |
| 140-149 | 100 | 100 | 100 | 99 | 87 | 77 | 67 | 55 | 42 | 32 | 21 | 11 | 5 | 2 | 0 |
| 150-159 | 100 | 100 | 100 | 100 | 90 | 80 | 70 | 58 | 45 | 34 | 22 | 12 | 5 | 2 | 0 |

First, 10 m wind components, 2 m temperature, and 2 m relative humidity are extracted from the NARR dataset and converted to GeoTiff files at 3-hour intervals from 1979 to 2019 (41 years). 10 m wind components were used to calculate 20 ft wind speed, in mph, and wind azimuth, in degrees. FFWI and MFFWI were then calculated at 3-hour intervals using the formulas presented above. Because rapidly spreading fires often cause significant damage in the first ~6 hours of a burn period, MFFWI values were averaged over a 6-hour period.

Next, the 6-hr average files were processed to determine the maximum 6-hr average MFFWI that occurred in a particular calendar day. Finally, for each 32 km by 32 km pixel in the NARR dataset, the ~15,000 (41 yr × 365 days/yr) daily maximum MFFWI values were sorted from high to low, with the date carried along and sorted analogously. These were then written to two (MFFWI and date) stacked GeoTiff rasters such that the first band contains the highest MFFWI value over 40 years and the date corresponding to the highest MFFWI. The second band contains the second highest MFFWI and date corresponding to that MFFWI, and so on.

With historical weather dates now identified, a 41-year (1979-2019) fire weather climatology was developed using the Weather Research and Forecasting (WRF) model to recreate historical days of fire weather significance across the analysis area. Approximately 200 days were included in this climatology, but for fire modeling purposes this data set was distilled to the most severe 50 days for a given location within the analysis area. High-resolution (1.2 km) hourly gridded fields of relative humidity, temperature, dead fuel moisture, and wind speed/direction were extracted from this analysis and provided as input to a Monte-Carlo-based fire modeling analysis.

5.4 Stochastic selection of ignition locations and wind/weather conditions

Reax generated GIS data depicting the locations of the four dams and the Klamath River. A 50-mile buffer was applied around these facilities data to create an “analysis area” where random ignitions are distributed within areas defined by the ignition mask layer (Figure 36). In the Monte-Carlo fire spread modeling analysis, 50% of the pixels within this buffer are ignited.

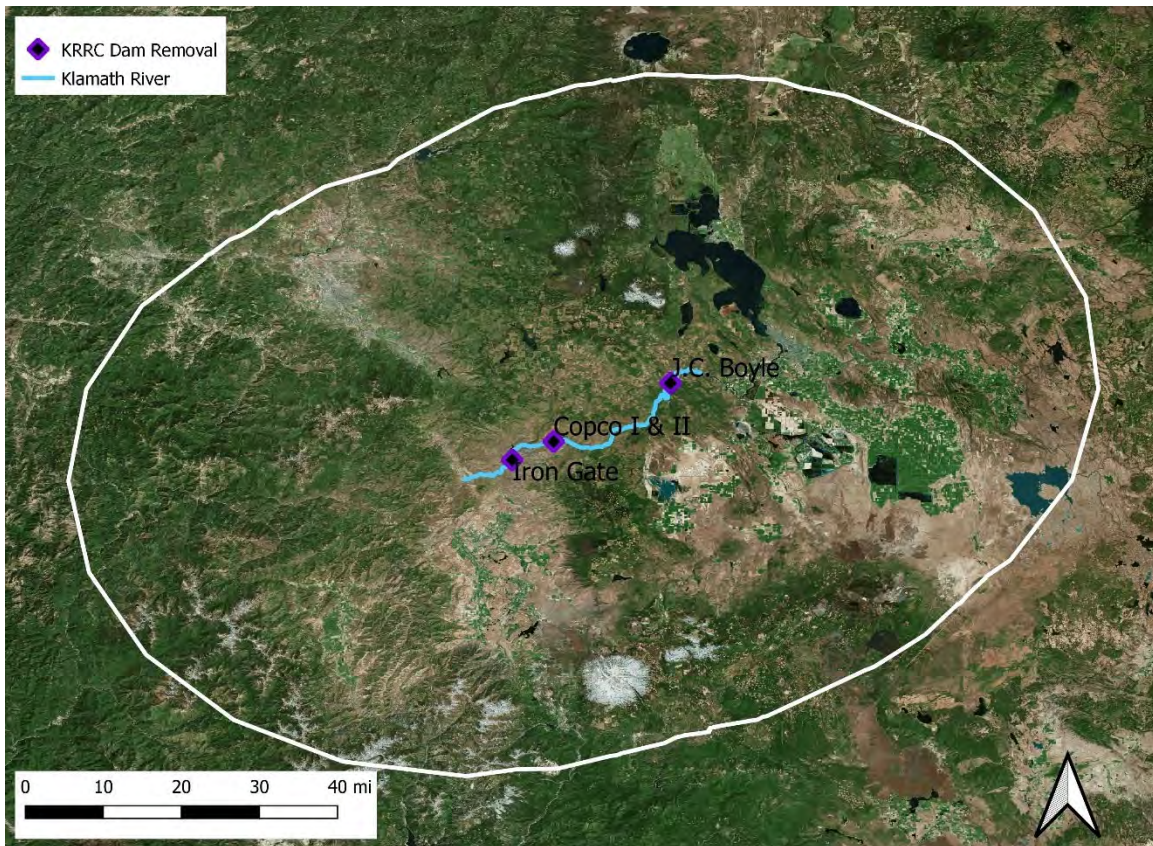


Figure 36. KRRC analysis area and ignition mask.

For each random ignition location, the weather stream is also selected randomly from the 50 most severe fire weather days (based on MFFWI) for that ignition location. Six hours of weather data, corresponding to approximately one burn period, are extracted from the fire weather stream and provided as input to the fire spread simulations.

5.5 Burn probability outputs

Burn probability is the likelihood that a point on the landscape will be impacted by fire during a given period of time, usually a year. By running ELMFIRE with stochastic ignition points and weather data burn probability for individual pixels can be determined. Providing the pre- and post-restoration fuel layers as input results in heatmaps of burn probability conditions before and after the removal of the dams and subsequent dewatering (Figure 37 - Figure 38). The primary region of change occurs in the reservoir basins where land previously covered by water was converted to vegetation. This change does not fundamentally alter the burn probability of the analysis area as a whole (Figure 39). Most importantly, regions with higher burn probability pre-restoration remain the same post-restoration and no new high burn probability regions are added. The burn probability calculated here does not incorporate MDS camera detections and therefore does not reflect any effect the cameras may have on burn probability.

This analysis will be updated to incorporate the detection and suppression effectiveness analyses described earlier in this report.

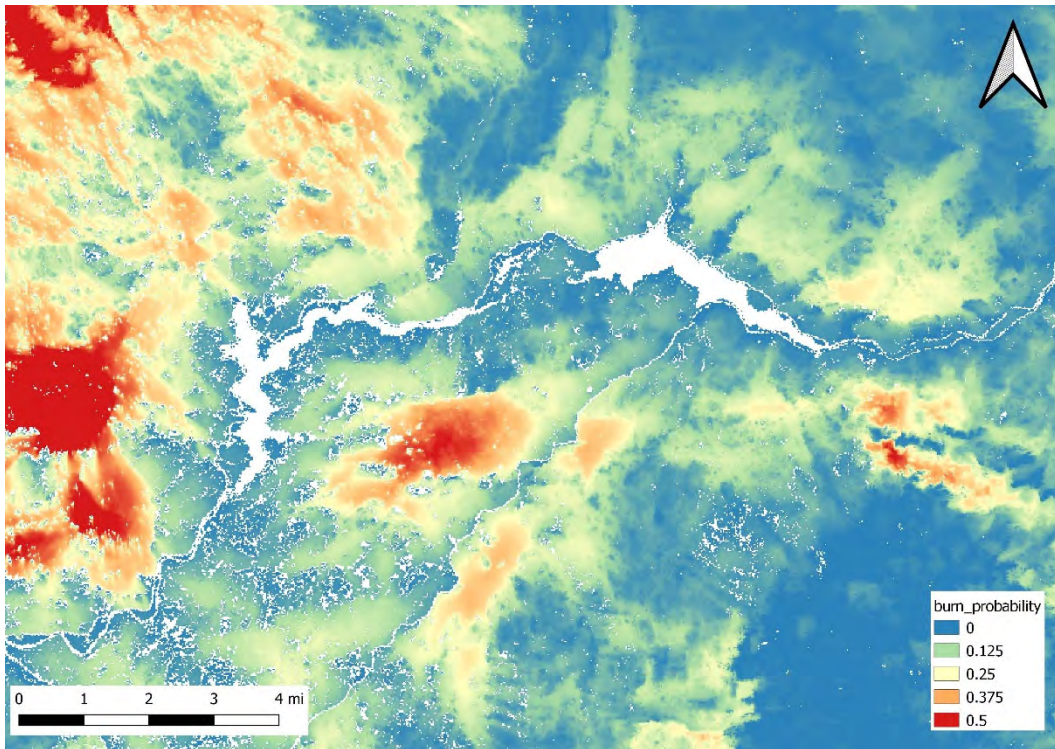


Figure 37. Pre-restoration burn probability.

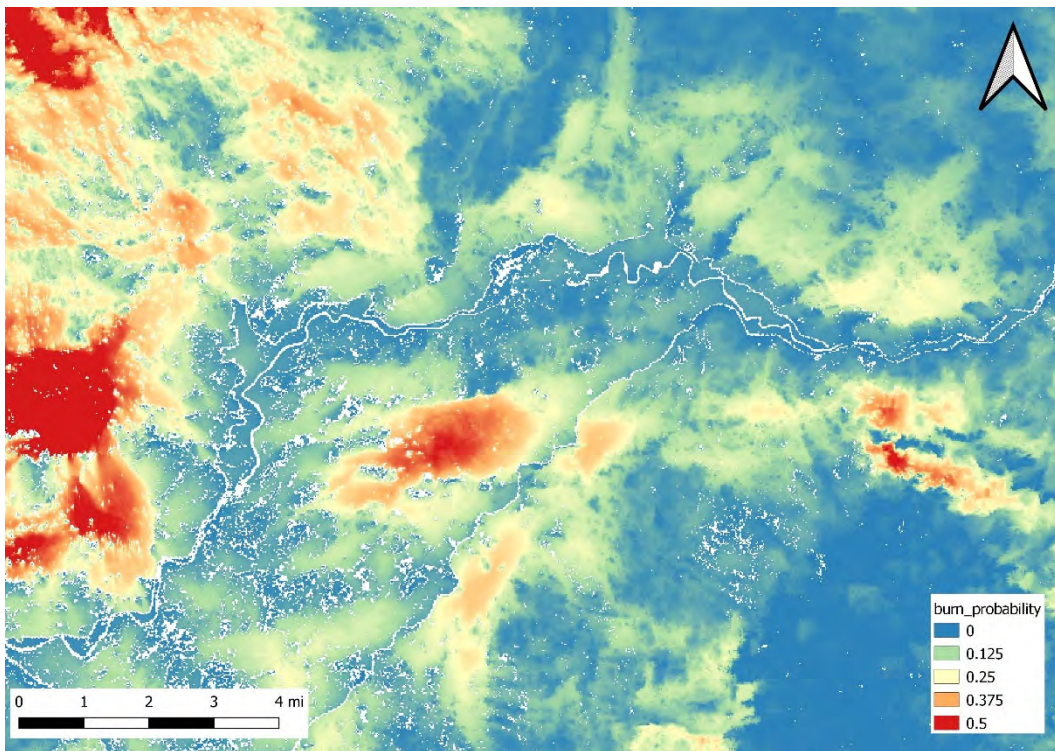


Figure 38. Post-restoration burn probability.

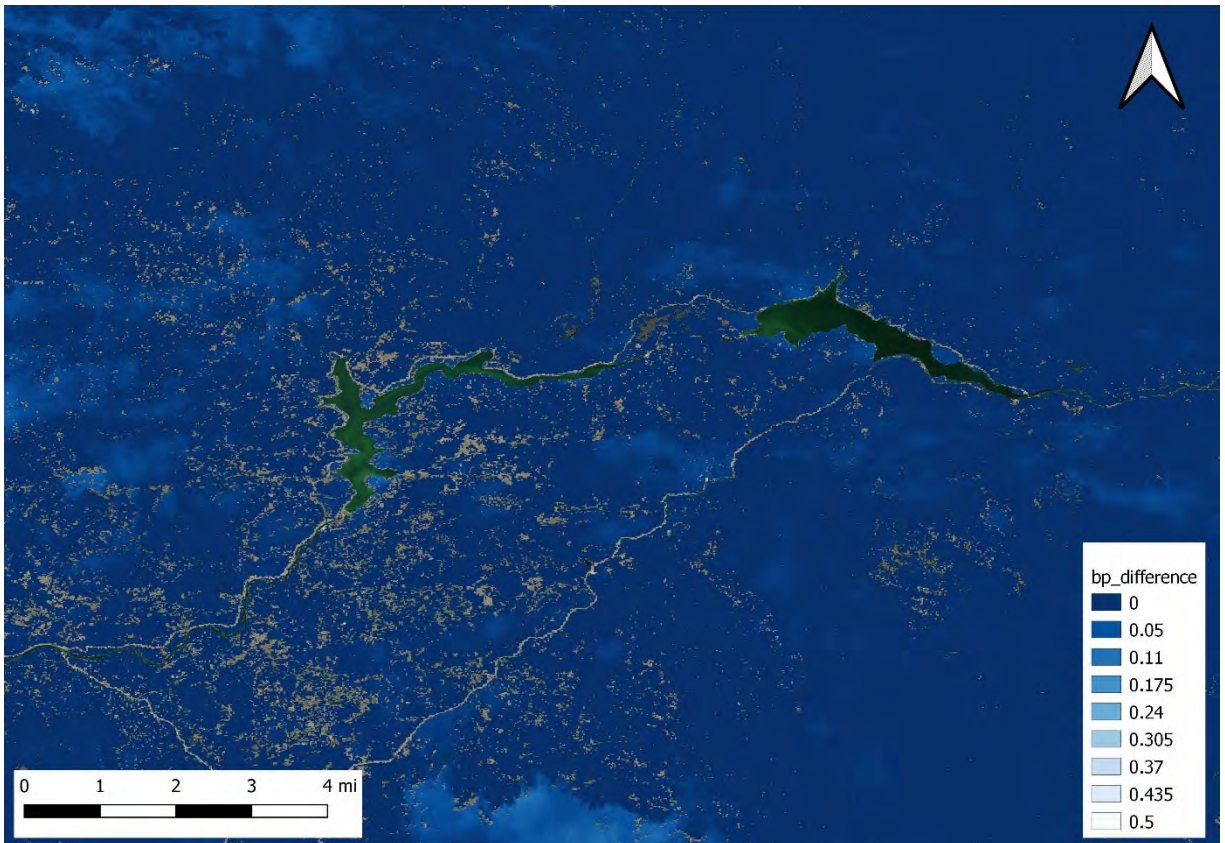


Figure 39. Difference between Pre- and Post-restoration burn probability.

6.0 CONCLUSIONS AND NEXT STEPS

The process of quantifying how the planned removal of four dams on the Klamath River will affect fire suppression capabilities and overall fire risk in the project area is ongoing. Despite the cumulative nature of the work, our analyses have led to some preliminary conclusions and recommendations:

1. Monte-Carlo fire spread modelling shows that dewatering of the project reservoirs and reclamation of approximately 1,000 acres of land will have a negligible effect on annual burn probability.
2. There will be no effective decrease in water availability for firefighting purposes following reservoir drawdown due to implementation of measures described in the November 2019 Draft Fire Management Plan. The convenience of the reservoirs may be impacted but the amount of water available should not be affected by dam removal. We recommend that portable water tanks be installed at several locations and are currently assessing whether installation of additional dry hydrants would be effective.
3. A viewshed analysis indicates that cameras will provide an effective means of early fire detection in the project area. Detection of most fires is expected at 0.1 acres or less. Installation of an additional camera on Mt. Ashland is recommended.

Moving forward, the ignition density maps and fire suppression methodology will be integrated with burn probability modelling. This analysis will be presented in the final report to be delivered in April 2020.

7.0 REFERENCES

- [1] Short, Karen C. 2017. Spatial wildfire occurrence data for the United States, 1992-2015 [FPA_FOD_20170508]. 4th Edition. Fort Collins, CO: Forest Service Research Data Archive. <https://doi.org/10.2737/RDS-2013-0009.4>
- [2] Abatzoglou, J. T., Balch, J. K., Bradley, B. A., Kolden, C. A., “Human-related ignitions concurrent with high winds promote large wildfires across the USA,” *International Journal of Wildland Fire* **27**: 377-386 (2018).
- [3] <https://frap.fire.ca.gov/frap-projects/fire-perimeters/>
- [4] https://rmgsc.cr.usgs.gov/outgoing/GeoMAC/historic_fire_data/
- [5] https://ftp.nifc.gov/public/incident_specific_data/
- [6] Draft Fire Management Plan Appendix 01, Klamath River Renewal Corporation, 2019.
- [7] <https://github.com/zoran-cuckovic/QGIS-visibility-analysis>
- [8] Cuckovic, (2016). Advanced viewshed analysis: A Quantum GIS plug-in for the analysis of visual landscapes. *Journal of Open Source Software*, 1(4), 32, doi:10.21105/joss.00032
- [9] <https://evsolutions.biz/hardware/>
- [10] <http://nhlr.org/nhlor.org/lookouts/us/ca/paradise-craggy-lookout/>
- [11] <http://nhlr.org/nhlor.org/lookouts/us/or/parker-mountain-lookout/>
- [12] <http://www.firelookout.com/or/chasemtn.html>
- [13] <http://nhlr.org/nhlor.org/lookouts/us/or/soda-mountain-lookout/>
- [14] <http://www.firelookout.com/or/ashland.html>
- [15] <http://www.alertwildfire.org/>
- [16] https://www.goes-r.gov/education/docs/fs_fire.pdf
- [17] <http://www.cstarsd3s.ucdavis.edu/systems/goes-efd/>
- [18] Rodrigues, M., Alcasena, F., Vega-Garcia, C., “Modeling initial attack success of wildfire suppression in Catalonia, Spain,” *Science of the Total Environment* **666**: 915-927 (2019).
- [19] Reimer, J., Thompson, D. K., Povak, N., “Measuring Initial Attack Suppression Effectiveness through Burn Probability,” *Fire* **2(4)**: 60 (2019).
- [20] Keane, R.E., Drury, S.A., Karau, E.C., Hessburg, P.F., and Reynolds, K.M., “A Method for Mapping Fire Hazard and Risk Across Multiple Scales and its application in fire management,” *Ecological Modeling* **221**: 2-18 (2010).
- [21] Finney, M.A., “FARSITE: Fire Area Simulator – Model Development and Evaluation,” United States Department of Agriculture Fore Service Rocky Mountain Research Station Research Paper RMRS-RP-4 Revised February 2004.
- [22] Tolhurst, K.G., Shields, B., and Chong, D., “Phoenix: development and application of a bushfire risk management tool,” *The Australian Journal of Emergency Management* **23**: 47–54 (2008).
- [23] Chong, D., Tolhurst, K., and Duff, T., “Incorporating Vertical Winds into PHOENIX RapidFire’s Ember Dispersal Model,” Technical Report, Bushfire CRC/University of Melbourne, 14 December 2012.
- [24] Chong, D., Tolhurst, K., and Duff, T., “PHOENIX RapidFire 4.0’s Convective Plume Model,” Technical Report, Bushfire CRC/University of Melbourne, 16 December 2012.
- [25] Chong, D., Tolhurst, K., and Duff, T., “PHOENIX RapidFire 4.0 Convection and Ember Dispersal Model,” Technical Report, Bushfire CRC/University of Melbourne, 16 December 2012.

- [26] Chong, D., Tolhurst, K., Duff, T., and Cirulis, B., “Sensitivity Analysis of PHOENIX RapidFire,” Technical Report, Bushfire CRC/University of Melbourne, 7 May 2013.
- [27] Sapsis, D., Brown, T., Low, C., Moritz, M., Saah, D., and Shaby, B., “Mapping Environmental Influences on Utility Fire Threat. A Report to the California Public Utilities Commission Pursuant to R.08 – 11-005 AND R.15-05-006,” Final Report, 16 February 2016.
- [28] Skamarock, W.C. and Klemp, J.B., “A time-split nonhydrostatic atmospheric model for weather research and forecasting applications,” *Journal of Computational Physics* **227**: 3465-3485 (2008).
- [29] <http://www.wrf-model.org/index.php>
- [30] <https://github.com/sig-gis/gridfire>
- [31] Morais, M.E., “Comparing Spatially Explicit Models of Fire Spread Through Chaparral Fuels: A New Algorithm Based Upon the Rothermel Fire Spread Equation,” MA Thesis, University of California at Santa Barbara, 2001.
- [32] Lautenberger, C., “Wildland Fire Modeling with an Eulerian Level Set Method and Automated Calibration,” *Fire Safety Journal* **62**: 289-298 (2013).
- [33] <http://reaxfire.com/trac/elmfire>
- [34] Decision Adopting a Work Plan for the Development of Fire Map 2 (Jan. 19, 2017) http://prccappiiswc002/Docs/CPUC-ElectricRegulations-Fire-ThreatMapsandFire-SafetyRegulations/Final-Decisions/CPUC/2017/CPUC-ElectricRegulations-Fire-ThreatMapsandFire-SafetyRegulations_Final-Dec_CPUC_20170119_D-17-01-009_399528.pdf
- [35] Lautenberger, C., “Mapping areas at elevated risk of large-scale structure loss using Monte-Carlo simulation and wildland fire modeling,” *Fire Safety Journal* **91**: 768 – 775 (2017).
- [36] Rothermel, R.C., “A Mathematical Model for Predicting Fire Spread in Wildland Fuels,” USDA Forest Service, Research Paper Int-115, January 1972.
- [37] Albini, F.A., “Estimating Wildfire Behavior and Effects,” USDA Forest Service General Technical Report Int-30, 1976.
- [38] Richards, G.D., “A General Mathematical Framework for Modelling Two-Dimensional Wildland Fire Spread,” *International Journal of Wildland Fire* **5**: 63-72 (1995).
- [39] Anderson, H.E., “Predicting wind-driven wild land fire size and shape,” United States Department of Agriculture Forest Service, Intermountain Forest and Range Experiment Station, Research Paper INT-RP-305, 1983.
- [40] Van Wagner, C.E., “Conditions for the Start and Spread of Crown Fire,” *Canadian Journal of Forest Research* **7**: 23-34 (1977).
- [41] Cruz, M. G., Alexander, M. E., and Wakimoto, R.H., “Development and testing of models for predicting crown fire rate of spread in conifer forest stands,” *Canadian Journal of Forest Research* **35**: 1626–1639 (2005).
- [42] Sethian, J.A., “A fast marching level set method for monotonically advancing fronts,” *Proceedings of the National Academy of Sciences* **93**: 1591-1595 (1996).
- [43] Rollins, M.G., “LANDFIRE: a nationally consistent vegetation, wildland fire, and fuel assessment,” *International Journal of Wildland Fire* **18**: 235-249 (2009).
- [44] <http://landfire.cr.usgs.gov/viewer/>
- [45] Scott, J.H. and Burgan, R.E., “Standard Fire Behavior Fuel Models: A Comprehensive Set for Use with Rothermel’s Surface Fire Spread Model,” United States Department of

- Agriculture Forest Service, Rocky Mountain Research Station, General Technical Report RMRS-GTR-15 (2005).
- [46] <https://www.fs.fed.us/pnw/fera/fft/fccsmodule.shtml>
- [47] National Centers for Environmental Prediction/National Weather Service/NOAA/U.S. Department of Commerce: NCEP North American Regional Reanalysis (NARR). Research Data Archive at the National Center for Atmospheric Research, Computational and Information Systems Laboratory. Dataset. <http://rda.ucar.edu/datasets/ds608.0/>.
- [48] Fosberg, M.A., “Weather in Wildland Fire Management: The Fire Weather Index,” *Conference on Sierra Nevada Meteorology*, American Meteorological Society, pp 1-4 (1978).
- [49] Simard, A.J., “The Moisture Content of Forest Fuels – 1. A Review of the Basic Concepts,” Canadian Department of Forest and Rural Development, Forest Fire Research Institute, Information Report FF-X-14, Ottawa, Ontario, 47 pp.
- [50] Goodrick, S.L., “Modification of the Fosberg fire weather index to include drought,” *International Journal of Wildland Fire* **11**: 205-211 (2002).
- [51] Schroeder, M.J., “Ignition probability,” USDA Forest Service. Fort Collins, CO. RMRS unpublished report, 1969.